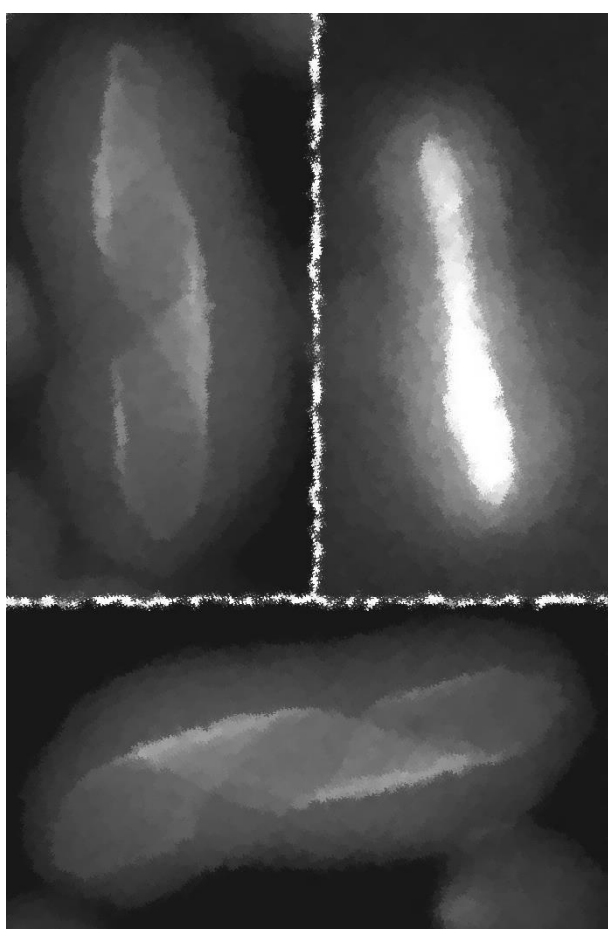# Silica-coated Anisotropic Semiconductor Nanocrystals as Building Blocks for Plastic Crystals

Eline M. Hutter

Masterthesis

Supervisors: dr. Francesca Pietra and Prof. dr. Daniël Vanmaekelbergh

CONDENSED MATTER AND INTERFACES

DEBYE INSTITUTE FOR NANOMATERIALS SCIENCE

UTRECHT UNIVERSITY

FEBRUARY 2014

Abstract

In this thesis, 1D and 2D anisotropic semiconductor nanocrystals are coated with silica in a reverse microemulsion to obtain water-soluble nanoparticles that are protected towards oxidation and photo-degradation. An extensive study on the effect of ammonia (which plays a catalytic role in the silica shell formation) on the resulting silica shell leads to a versatile method that can be widely used to coat anisotropic nanocrystals with a uniform and size-tunable silica shell. Furthermore, modification steps are explored to use these silica-coated semiconductor nanocrystals as building blocks for long-range liquid crystals, better known as plastic crystals. In this respect, it is essential to obtain long-range interparticle repulsion, which can be achieved by charge-stabilization of the nanoparticles. Therefore, the silica-coated nanocrystals are functionalized with an organic ligand and consequently transferred to a nonpolar solvent. The challenge however remains to measure these nanometer-sized objects when these are dispersed in a liquid medium, which is needed to detect plastic crystal phases.

Contents

1. Introduction

Recently, long-range liquid crystals of freely rotatable colloidal dumbbell-shaped microparticles have been developed,[1–7] better known as plastic crystals. Given that the orientation of the dumbbells is sensitive towards external electric fields, plastic crystals are very interesting in terms of switchable photonic crystals. The building blocks for the currently developed plastic crystals were amorphous micrometer-sized colloids. However, it would be interesting to investigate whether the characteristics of plastic crystals could be combined with the remarkable physical properties of nanometer-sized crystalline semiconductors. For instance, long-range liquid crystals of semiconductor nanocrystals that are highly luminescent in the visible could be of interest both from a fundamental point of view and in terms of applications, such as optoelectronic or lighting devices.[8]

Dense-packed as well as liquid crystals of semiconductor nanocrystals have already been extensively studied,[9–17] however these systems consist of close-packed structures, in which there is no rotational freedom and hence the orientation of the nanocrystals is fixed. This could be a limiting factor in making optimal use of certain properties, e.g. the ability of anisotropic CdSe/CdS core/shell NRs to emit linearly polarized light is only useful if these are aligned. In this respect, these are of special interest to be used for plastic crystals as their internal dipole moment allows them to be aligned into the same direction when an electric field is applied.

The aim of this work is to design different types of semiconductor nanocrystals as building blocks for plastic crystals, starting with CdSe/CdS core/shell NRs. Prior modification steps are required to protect the as-synthesized nanocrystals towards oxidation and induce sufficient interparticle repulsion to obtain long-range crystals. In this respect, the nanocrystals are first coated with silica and afterwards functionalized with an organic compound via different routes.

Theoretic background necessary for understanding of this thesis will be given in chapter 2. Chapter 3 presents a detailed study on the incorporation mechanism of different anisotropic nanocrystals in silica, which finally results in a general method to coat anisotropic nanocrystals with a uniform silica shell. Chapter 4 explores the design and characterization of silica-coated rod-shaped nanocrystals as building blocks for plastic crystals, resulting in negatively charged nanoparticles dispersable in nonpolar solvents.

2. Theory

The first part of this chapter introduces the main properties of colloidal semiconductor nanocrystals (NCs) and discusses their size- and shape-dependence, followed by a description of the incorporation of NCs in a silica shell. The last part deals with theoretic background necessary for basic understanding of plastic crystals, a possible application of these silica-coated NCs.

2.1 Colloidal semiconductor nanocrystals

NCs are nanometer-sized crystalline structures with features in between those of a molecule and the bulk material with size-dependent magnetic, electronic and optical properties.[18] Colloidal semiconductor NCs show unique size- and shape-dependent physical properties due to quantum and dielectric confinement (paragraph 2.1.1).[18–20] Isotropic colloidal semiconductor NCs display confinement in three dimensions, while in colloidal semiconductor NCs with anisotropic shapes this can be reduced to only one or two dimensions (paragraph 2.1.2). In general, NCs can be coated with one or multiple shells of different semiconductor materials for both protection and extension of optoelectronic properties (paragraph 2.1.3).[12,21–24] In particular, the incorporation of NCs in an inert wide band gap material such as silica shields them both physically and chemically from the direct environment while the optoelectronic properties are preserved (paragraph 2.1.4).[25–27]

2.1.1 Size-dependent optical properties

Colloidal semiconductor NCs are commonly synthesized by the hot injection method, yielding ligand-stabilized NCs.[21] The organic ligands are often amphiphilic: the polar groups coordinate to the metal atoms on the surface of the NCs and the nonpolar hydrocarbon tails enable the NCs to form stable colloidal dispersions in nonpolar solvents. Furthermore, these organic capping ligands affect the growth kinetics of NCs and hence control their size and shape (2.1.2), which are both important for their optoelectronic properties. This can be explained considering two main effects that occur if semiconductors enter the nanometer size regime: (i) quantum confinement and (ii) a relatively large surface-to-volume ratio compared to the bulk material.

Quantum confinement

In general, an important electronic feature of semiconductor materials is the intrinsic band gap between valence and conduction band, with an energy separation in the order of a few electron volts.[28] The bulk material is here considered as a huge molecule with an indefinite number of bonding and antibonding molecular orbitals, in which molecular orbitals that are closely spaced in energy form a quasi-continuum of energy levels: an energy band.[29] Whereas a molecule has discrete energy levels, the valence band (VB) and the conduction band (CB) of a semiconductor consist of a quasi-continuum of bonding and antibonding molecular orbitals, respectively. Hence, electrons from the completely filled VB can be thermally excited to the CB, thereby leaving a hole with net positive charge in the VB. This electron-hole pair is delocalized throughout the semiconductor and called an exciton. A measure for the average distance between electron and hole is the spatial extension, which is defined by the exciton Bohr radius (a_0).[21] The value of a_0, typically in the range of 1 to 100 nm, depends on several parameters and is therefore characteristic for the type of material. If a semiconductor itself is smaller than its a_0 ($d \leq 4a_0$) the exciton is spatially confined, increasing the energy of the band gap and causing distinct energy levels. These so-called quantum confinement effects play a vital role in the optical and electronic properties of semiconductor NCs, better known as quantum dots (QDs),[18,19,30] which have both discrete energy levels and energy bands. Considering the electronic structure of semiconductor NCs from the evolution of the molecular orbitals from molecule to bulk gives insight in their size-dependent energy levels, which is represented schematically in Figure 2.1.
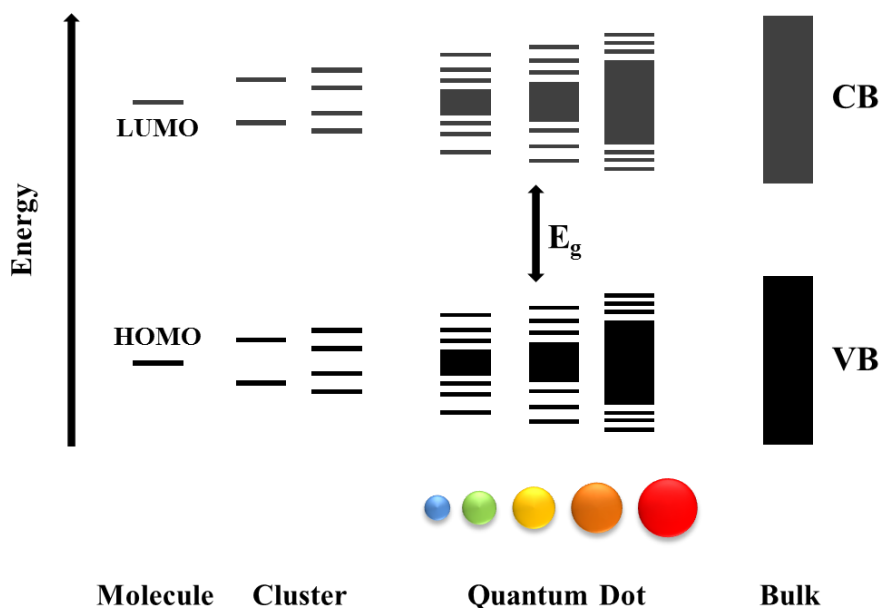
Figure 2.1: Schematic representation of the size-dependent evolution of the energy levels from molecule to bulk. LUMO denotes the lowest unoccupied molecular orbital, HOMO the highest occupied molecular orbital. The grey continuum of levels represents the conduction band, whereas the valence band is drawn in black. In the ground state, the valence band is completely filled with electrons while the conduction band is empty. The spheres display the size-dependent emission colors of quantum dots, which depends on the extent of the band gap.

The fact that the energy levels remain discrete at the edges of the bands can be explained in terms of the density of states of an energy band: the energy versus the number of states with that energy. As displayed in Figure 2.2, both for the VB and the CB the density of states is the highest in the middle of the energy band. The number of levels decreases towards the edges. If the size of a bulk semiconductor decreases towards the nanometer regime, energy levels are removed throughout the entire band gap. Consequently, there is a higher probability that energy levels are removed from the edges of the band gap than from the middle of the band gap (because at the edges there were fewer states to start with). Therefore, the band gap energy E_g of QDs is larger than that of the bulk semiconductor and furthermore the discrete energy levels will be at the edges of the bands.
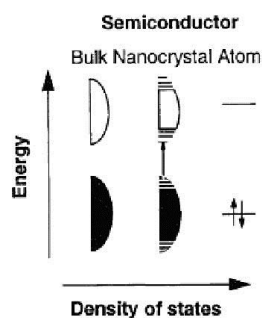
Figure 2.2: Energy versus density of states of a semiconductor. The valence band, which is completely filled with electrons in the ground stated, is represented in black, whereas the conduction band is white. This image shows that most energy levels are positioned in the middle of an energy band. As mentioned in the text, in a semiconductor nanocrystal there are not enough levels to form a complete band, hence the levels at the edges will remain discrete. Reproduced from Ref. 18.

Optical properties and contribution of the surface

The optical properties of semiconductor NCs are highly dependent on their electronic structure,

determined by both the intrinsic E_g of the bulk material and the size of the semiconductor NCs (due to quantum confinement effects). By absorption of a photon with energy larger than the band gap, a localized exciton is created by excitation of an electron from the VB to the CB. When the electron and hole recombine radiatively, a photon is emitted through a process called photoluminescence (PL). The PL wavelength corresponds to the energy separation between the highest level of the VB and the lowest level of the CB, i.e. the band gap of the semiconductor NCs. The excess photon energy is lost as heat by non-radiative relaxation to the lowest level of the CB. The size dependence of these optical properties is displayed in the position of both the absorption and emission peak: these transitions shift to higher energies (i.e. lower wavelengths) as the QDs decrease in size. Furthermore, the shape of the absorption and PL spectra provides valuable information on the size distribution of the QD dispersion, for instance a narrow emission transition indicates a narrow size distribution of the QDs.

Not only the size distribution affects the optical properties, but also the surface plays an important role. Due to the relatively large surface-to-volume ratio, a QD has a significant number of its atoms on the surface. These surface atoms are highly reactive due to the lack of nearest neighbors and the so-called dangling bonds that subsequently stick out of the surface. Furthermore, the efficiency of radiative recombination of the exciton depends strongly on the surface construction of a QD. That is, if there are defects on the surface (e.g. missing atoms or impurities such as ligands or halogen atoms), excited electrons or holes can be trapped and hence not recombine efficiently. These trap states quench the emission and hence limit the overall performance of the QDs.

2.1.2 Anisotropic semiconductor NCs

As mentioned in the previous paragraph, the characteristic properties of semiconductor NCs are mainly attributed to the spatial confinement of the exciton. QDs are more or less isotropic in shape; therefore the exciton is confined in three dimensions. However, for anisotropic semiconductor NCs it could be that the confinement is reduced to only one or two dimensions, which affects the electronic structure.[19,20,31] For instance, in rod-shaped semiconductor NCs the exciton is confined in two dimensions as only the length exceeds a_0.[32–34] The electronic structure therefore differs from the isotropic QD that was discussed in the previous paragraph. Sheet- or platelet-shaped semiconductor NCs have quantum confinement only in one dimension and are conventionally referred to as 2D materials, since the lateral dimensions are considered to be infinite compared to the thickness.[35–40] Similarly, rod-shaped NCs and QDs are referred to as 1D and 0D, respectively. Figure 2.3 shows the evolution of the density of states from the 3D bulk crystal to a 0D QD.
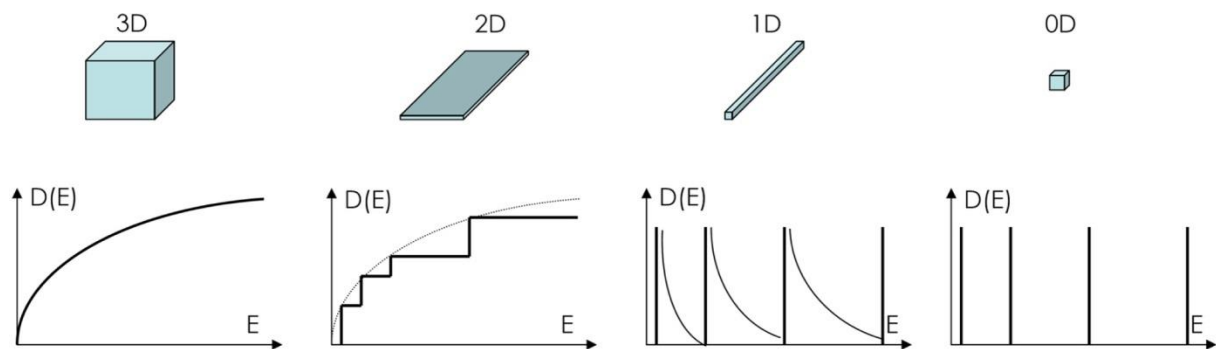
Figure 2.3: Evolution of density of states from bulk (3D) to QD (0D), in which platelets (2D) and rods (1D) have an electronic structure intermediate to the two extremes that were elucidated in the previous paragraph. Reproduced from Ref. 31.

2.1.3 Core-shell HNC structures

In general, NCs can be combined together with another crystalline material for protection, extension of optoelectronic properties and shape design,[12,21–24,41,42] resulting in so-called heteronanocrystals

(HNCs). A specific HNC type is a core-shell structure, comprising a core surrounded by one or multiple shells. The electronic structure of HNCs that consist of multiple semiconductor materials depends on the band alignment between the semiconductor materials, which can be classified in three different types: Type I, Type I$^{\frac{1}{2}}$ and Type II. These are represented schematically for core-shell HNC structures in Figure 2.4.[21] In Type I, the band gap of the shell is (much) larger than the one of the core and the electron wavefunction (denoted by 'e') as well as the hole wavefunction (denoted by 'h') remain confined in the core. In Type II, the semiconductor shell has its lowest level of the CB at lower energy than the CB of the core. Consequently, after excitation the electron wavefunction is delocalized in the shell and is spatially separated from the hole wavefunction, which remains in the core. Type I$^{\frac{1}{2}}$ is intermediate to the others, i.e. the hole wavefunction is confined in the core whereas the electron wavefunction is delocalized throughout the entire HNC.
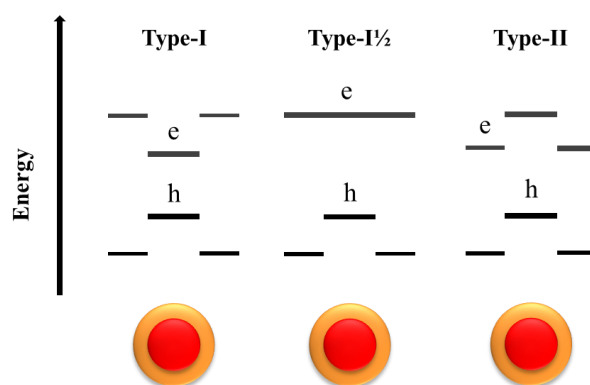
Figure 2.4: Relative band alignments for different types of core-shell structures. The inner lines correspond to the core, the outer lines to the shell. The electron and hole wavefunctions are denoted by 'e' and 'h', respectively.

Core-shell NCs are generally obtained in two steps, first the cores are synthesized and afterwards another NC type nucleates heterogeneously on the cores. Heterogeneous nucleation requires less energy than homogeneous nucleation, therefore using a lower growth temperature enables to selectively grow shells around the cores: this is known as seeded growth.

In this thesis, a specific core-shell structure will be used, which consists of two semiconductor materials: a wurtzite cadmium selenide (CdSe) hexagonal QD embedded in a cadmium sulfide (CdS) shell nanorod (NR).[22,43] These are synthesized by seeded growth, using an organic ligand (i.e. octadecyl phosphonic acid (ODPA)) that binds most strongly to the facets parallel to the z-axis of the NR and hence promotes growth along the z-axis. This results in a pencil-shaped CdS rod with the CdSe core located close to the flat end, as sketched in Figure 2.5. The length of these NRs depends on both the reaction time and the concentration of sulfur precursor relative to the concentration of the cores: a longer reaction time and a higher precursor-to-core concentration lead to longer NRs and vice versa.
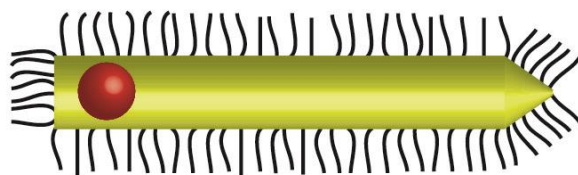
Figure 2.5: Schematic representation of a CdSe/CdS core/shell NR, in which the core (red) is embedded in a pencil-shaped rod (yellow), stabilized by ODPA (black). Note that, the CdSe core has a wurtzite (hexagonal) crystal structure and is therefore not spherical.

This type of CdSe/CdS core/shell NRs have drawn extensive attention in the past decade due to their many possible applications (e.g. self-assembly, photo catalysis), characteristic electronic structure and well-defined surface construction.[9,13,43–47] Given that a CdSe/CdS HNC has a type I½ band-offset, the hole wavefunction is confined in the CdSe core while the electron wavefunction is delocalized throughout the CdS shell.[48] Therefore, emission originates from the CdSe core whereas the absorption of photons is dominated by the CdS shell, resulting in relatively high quantum yields.[31] Furthermore, if CdSe/CdS (or CdSe) NRs are aligned, these emit linearly polarized light along the alignment direction.[12,49]

2.1.4 Encapsulation of colloidal semiconductor nanocrystals in a silica shell

A major drawback of colloidal semiconductors in applications such as fluorescent biolabels[50] or light-emitting devices[51] is their poor stability in water- and oxygen-rich environments. A possible strategy to deal with this problem is the encapsulation in an inert shell that shields the materials both chemically and physically from the direct environment. In this respect, the incorporation of colloidal NCs in a wide band gap material such as silica (SiO_2) is highly interesting, because it increases the photochemical stability while the optical properties are preserved.[52] Furthermore, the silica shell can easily be functionalized with organic ligands.[27,53–56] This allows the NCs to be dispersed in both polar and nonpolar solvents, which largely increases their processability. In the past decades, extensive work has been done on the incorporation of QDs in silica.[26,27,41,52,54,57–64] The two main approaches to coat nanoparticles (NPs) with a silica shell are the traditional Stöber method[65,66] and the so-called reverse microemulsion method.[25,67–69] Although the Stöber method is highly effective in growing silica shells around microparticles[66] or metal NPs,[55] it does not yield uniform silica shells on single semiconductor NCs.[70] The reverse microemulsion method however allows for the incorporation of single QDs located exactly in the middle of silica spheres. In this approach, the silica shells grow around single QDs that are individually trapped inside an aqueous micelle of a water-in-oil (w/o) microemulsion. The continuous phase of the reverse microemulsion is cyclohexane, which is mixed with a surfactant, the QDs and silica precursor molecules. The silica nucleation and growth are catalyzed by the basic environment resulting from the addition of an aqueous ammonia solution. Despite of the comprehensive work on the silica coating of QDs, there are only a few studies reporting the encapsulation of anisotropic NCs with the reverse microemulsion method.[71–75] The encapsulation of anisotropic semiconductor NCs with silica is beneficial for their potential in plastic crystals, but also for other shape-dependent applications such as shape-directed self-assembly[76,77] or antibody specificity for cellular uptake.[78,79] In this respect, preservation of the anisotropic shape is a requisite. However, the incorporation of NRs in silica with the reverse microemulsion method caused a drastic decrease in the particles' aspect ratio as the shape changes into dumbbells and ellipsoids.[71–73] Moreover, silica shells thinner than 10 nm cannot be obtained with the currently available methods.

2.2 Plastic crystals

A plastic crystal is considered as a liquid crystal phase, either in two or three dimensions, in which the particles have positional order but rotational freedom due to the relatively large interparticle distance. Orientationally disordered liquid crystal were experimentally obtained for spherical[80–82] and recently also for dumbbell- and rod-shaped microparticles dispersed in nonpolar solvents.[1–3,5,6] In the case of anisotropic particles (as opposed to perfect spheres), the rotational freedom results in orientational disorder and hence the particles are randomly orientated. It would be interesting to design plastic crystals with silica-coated semiconductor NCs such as CdSe/CdS core/shell NRs, since the disoriented NRs are then expected to become aligned into the same direction when an electric field is applied and consequently be able to emit linearly polarized light.

In this respect, it is essential that the lattice constant exceeds the largest dimension of the anisotropic

particles to prevent interparticle collisions upon rotation. Therefore, the electric double layers of the particles should be much larger than the particles themselves, inducing long-range repulsion. To obtain a plastic crystal, equilibrium between attractive and repulsive forces needs to be achieved. The next paragraphs describe how the electric double layer affects the interparticle distance and how this is measured (2.2.1) followed by calculations on the packing density of plastic crystals (2.2.2).

2.2.1 Long-range repulsion and the ζ-potential

In plastic crystals, long-range repulsion is often achieved by charge stabilization. The attractive van der Waals forces can be reduced by refractive index matching of particles with the solvent.[5] The extent of the double layer mainly depends on the ion concentration in the solvent affecting the Debye screening length and the particles' surface charge.[81] The electrostatic surface potential, better known as the ζ-potential, is a measure of the (electro-kinetic) charge between colloidal particles and the surrounding medium and hence serves as an indication of the repulsion between the particles.[83,8485] The ζ-potential is calculated from the electrophoretic mobility μ_e, which can be experimentally obtained with electrophoretic light scattering measurements. For a medium with vanishing ionic strength (i.e. nonpolar solvent with low dielectric constant ε), in which the electric double layer of a particle is larger than its radius, ζ is calculated from μ_e by the Hückel approximation (equation 1).[85,86] The viscosity η and the dielectric constant ε depend on the type of solvent.

$$\zeta = \frac{1.5 \eta \mu_e}{\varepsilon \varepsilon_0} \tag{1}$$

It was found that a ζ-potential of approximately 40 mV (thermal voltage $k_BT/e \approx 26$ mV at room temperature) is sufficient to obtain a charge-stabilized dispersion and hence induce the formation of a plastic crystal.[81,86,87]

2.2.2 Packing density in plastic crystals

Whereas crystallization of (anisotropic) colloids usually requires a high packing density,[88–92] for plastic crystals the packing fraction needs to be relatively low to obtain rotational freedom and prevent interparticle collisions. The packing fraction ϕ can be calculated from geometric relations and converted to the weight percentage (wt%) of a dispersion. In this thesis, the silica-coated NRs (chapter 4) with length l and diameter d are considered as prolate spheroids with volume V_{NR}:

$$V_{NR} = \frac{4}{3}\pi \frac{d}{2}\frac{d}{2}\frac{l}{2} = \frac{\pi d^2 l}{6} \tag{2}$$

If these form an fcc structured plastic crystal, i.e. four particles per unit cell with lattice constant a, the volume packing fraction is given by:

$$\phi = \frac{4V_{NR}}{a^3} = \frac{2\pi d^2 l}{3a^3} \tag{3}$$

For an fcc crystal structure, the shortest interparticle distance (center-to-center) is given by $R = \frac{\sqrt{2}}{2}a$, therefore the volume fraction is expressed in terms of R as follows:

$$\phi = \frac{\sqrt{2}\pi d^2 l}{6R^3} \tag{4}$$

If the densities of the particles and the solvent are taken into account, the volume fraction can be translated to the wt% of a dispersion. This is a measurable quantity and can hence be used to experimentally obtain plastic crystals with the desired interparticle distance.

3. Silica coating of anisotropic semiconductor nanocrystals*[1]

3.1 Introduction

As mentioned in paragraph 2.1.4, silica coating with the reverse microemulsion method[25,67–69] has been most successful for the formation of silica spheres with individual QDs located exactly in the middle. The incorporation of hydrophobic colloidal QDs in silica with the reverse microemulsion method was first proposed by Selvan *et al*.[25,60] The incorporation mechanism is explained in terms of a ligand exchange between the hydrophobic capping molecules on the surface of the QDs and the silica precursor tetraethoxysilane (TEOS), prior to silica growth.[27,68] While the early studies on the mechanism suggest the possibility of silica growth after the formation of a surfactant bilayer,[68] later experiments exclude this idea by confirming the presence of hydrolyzed TEOS on the surface of the QDs,[27] which also declares that the originally hydrophobic NCs can be trapped in the micelles containing an aqueous phase. This method is not effective to incorporate QDs with thiolated ligands (without further modifications) in silica spheres. The fact that this process is sensitive towards the type of the original capping molecules gives evidence to the idea that ligand exchange is an essential step. Only recently, silica coating with the reverse microemulsion method was successfully applied to anisotropic NCs like tetrapods[74,75] and NRs.[71–73] A detailed study on the incorporation of CdSe/CdS core/shell NRs revealed that for these anisotropic NCs, the ligand exchange and hence the silica growth starts at the most reactive crystallographic facets.[72] In this work, these results are reproduced and more insights are obtained as the variation of certain parameters leads to different silica growth behavior. The hydrolysis and condensation rates of the silica precursor are tuned by varying the ammonia concentration in the aqueous phase of the reverse microemulsion.[93] The effect on the resulting silica shell is studied in detail for CdSe/CdS core/shell NRs (3.4.1). The results not only confirm the proposed mechanism of ligand exchange, but also provide more insights on the growth of silica at anisotropic NCs with different crystallographic facets. Further, highly anisotropic 2D NPLs are incorporated in silica under varying ammonia concentrations (3.4.3 & 4). The final morphologies and optical properties of different silica-coated anisotropic semiconductor NCs are discussed followed by a proposed incorporation mechanism. Finally, a general discussion and conclusion on the silica coating of anisotropic NCs are presented as a starting point for further research (3.5 & 6).

3.2 Experimental

This paragraph deals with the experimental details regarding the syntheses of CdSe/CdS core/shell NRs, CdSe NPLs, CdSe/CdS core/shell NPLs and the incorporation of these materials in silica. The resulting silica-coated NCs are soluble in polar solvents such as water and ethanol. If the silica-coated NCs are further functionalized with a hydrophobic organic compound such as octadecyltrimethoxy-silane (OTMS), these can be dispersed in nonpolar solvents. Different routes to obtain hydrophobic silica-coated NCs will be elucidated in chapter 4. The NPLs used in this chapter were synthesized by Dariusz Mitoraj.

3.2.1 Materials

3.2.1.1 Chemicals

Ammonia (29.9 wt% in water, Sigma-Aldrich, stored at 7°C), bis(trimethylsilyl)sulfide (TMS$_2$S, Sigma-Aldrich), cadmium acetate (Cd(Ac)$_2$, Sigma-Aldrich, 99.99%), cadmium acetate dihydrate (Cd(Ac)$_2$(H$_2$O)$_2$, Sigma-Aldrich), cadmiumoxide (CdO, Sigma-Aldrich, 99%), dodecylamine (DDA, Sigma-Aldrich, 98%), gold(III)chloride hydrate (HAuCl$_4$, Sigma-Aldrich), octa-decyl-phosphonic acid (ODPA, Sigma-Aldrich, 97%), oleic acid (OA, Sigma-Aldrich), poly(5)oxyethylene-4-nonylphenyl-

---

ether (NP-5, IgePAL CO 520, Sigma-Aldrich), selenium (Strem Chemicals, 99.99%), sulfur (Alfa Aesar, 99%), tetraethyl orthosilicate (TEOS, Sigma-Aldrich, 99%), trioctylphosphine (TOP, Sigma-Aldrich, 90%), and trioctylphosphine oxide (TOPO, Sigma-Aldrich, 99%) were used for the synthesis of the NPs.

3.2.1.2   *Solvents*

Acetone (Merck, anhydrous), butanol (Sigma-Aldrich, anhydrous, 99.8%), cyclohexane (Sigma-Aldrich, anhydrous, 99%), ethanol (Alfa Aesar, anhydrous, 96%), hexane (Sigma-Aldrich, anhydrous, 99.8%), methanol (Sigma-Aldrich, anhydrous, 99.8%), and toluene (Sigma-Aldrich, anhydrous, 99.8%) were used as supplied.

3.2.2   Synthesis of CdSe seeds

The CdSe NC seeds were synthesized according to the hot injection method reported by Carbone *et al.*[12] TOPO (3.0 g), ODPA (0.290 g) and CdO (0.060 g) were mixed in a 50 mL three-neck flask and heated to 150°C under vacuum. After 2 h, the solution was heated to 330°C under nitrogen until Cd-ODPA complexes were formed, indicated by transparency of the solution. Next, TOP (1.5 g) was injected followed by heating to 350-370°C and injection of TOP-Se (0.058 g Se in 0.360 g TOP). The reaction was quenched by removal of the heating source, cooling down by blowing air towards the flask and finally addition of 5 mL toluene as the temperature dropped below 90°C. The final size of the NCs depends on the reaction time: longer growth leads to larger NCs. The obtained CdSe NCs were washed three times with methanol, redispersed in toluene and stored under nitrogen in a glovebox.

3.2.3   Synthesis of CdSe/CdS core/shell NRs

The CdSe/CdS core/shell NRs were synthesized using a seeded growth approach.[12] TOPO (3.0 g), ODPA (0.330 g) and CdO (0.090 g) were heated to 150°C in a 100 mL three-neck flask in a Schlenk-line under vacuum for 2 h. Afterwards, the solution was heated to 350°C to form Cd-ODPA complexes and TOP (1.5 g) was injected. Once the temperature was stabilized, TOP-S (0.12 g S in 1.5 g TOP) and 200 μL CdSe NC seeds in TOP (400 μM) were rapidly injected. After 12 minutes, the reaction was quenched and washed by precipitation/redispersion with methanol and toluene. Finally, size selective precipitation was performed by adding 5 mL toluene and 500 μL methanol followed by centrifugation for 5 minutes at 1800 rpm. The precipitated NRs were dispersed in 5 mL toluene and stored in a glovebox.

3.2.4   Synthesis of gold-tipped CdSe/CdS core/shell NRs

Preparation Au stock solution HAuCl$_4$ (3.1 mg) was dissolved in H$_2$O (6 mL) and mixed with DDA (960 μL) dispersed in toluene (6 mL) under vigorous stirring (1 min.). The resulting solution was left until phase separation occurred, allowing the gold to transfer from the aqueous to the organic phase (toluene). Afterwards, the organic bottom phase (dark yellow) was isolated and stored.

Photo-induced deposition of Au on CdSe/CdS core/shell NRs 78 μL of a solution of NRs (16 μM) was diluted with 1 mL toluene and 250 μL methanol was added followed by addition of 1 mL of the Au stock solution under vigorous stirring. Then, the solution was placed under UV irradiation using a 6 W Portable 365 nm UV-lamp as light source. After 10 minutes, the solution was removed from the UV source and the reaction was quenched by the addition of methanol. The gold-tipped NRs were washed twice by precipitation/redisperion with methanol and toluene.

3.2.5   Synthesis of CdSe NPLs

The CdSe nanoplatelets were synthesized according to Ithurria *et al.* (Protocol 1).[37] Cd(Ac)$_2$ (240 mg), oleic acid (285 μL) and octadecene (15 mL) were mixed in a three-neck flask and degassed at 80°C under vacuum for 1 h. Then, the mixture was heated to 200°C and 150 μL of 1M TOP-Se was

injected. After 1 h the reaction was quenched and CdSe NPLs were washed twice with a methanol/butanol mixture (1:3 by volume) and stored in 5 mL hexane.

3.2.6 Synthesis of CdSe/CdS core/shell NPLs

The CdSe/CdS core/shell nanoplatelets were synthesized via layer-by-layer growth reported by Mahler *et al.*[23] Therefore, 1.2 mL of the CdSe nanoplatelets solution was diluted in 1.2 mL hexane and 50 µL of bis(trimethylsilyl) sulfide (TMS$_2$S) was added. After 1 h, the color changed from yellow to orange. The obtained NCs were washed twice with ethanol and redispersed in hexane. Then, 20 mg of Cd(OAc)$_2$(H$_2$O)$_2$ was added and another color shift from orange to red was observed as the mixture was sonicated for 10 mins. The disaggregation was induced by addition of 200 µL of oleic acid. The NPLs were finally washed with ethanol and redispersed in hexane.

3.2.7 Silica coating of NCs by the reverse microemulsion method

The CdSe/CdS core/shell NRs were coated with silica according to the method described by Pietra *et al.*[72] The reverse microemulsions were prepared by dispersion of 1.3 mL NP-5 in 10 mL cyclohexane, followed by the addition of 1-2 nmol NRs in toluene and afterwards 80 µL TEOS. The solutions were continually stirred and there were at least fifteen minutes between all additions. Finally, 150 µL ammonia solution was added after which the solution was stirred for one more minute and then stored. The reactions were quenched by addition of ethanol followed by three sedimentation/redispersion cycles. The resulting silica-coated NRs were stored in 10 mL ethanol. The encapsulation of the NPLs in a silica shell was performed in a similar manner, by adding variable amounts from stock solutions with OD of 0.26 and 0.20 for CdSe NPLs and CdSe/CdS NPLs (in 80 times diluted solution, measured at 400 nm), respectively. The type and amount of NCs added to each microemulsion are presented in Appendix C. Different ammonia solutions were prepared by dilution of a stock solution with water, resulting in a series of concentrations from 29.9 wt%, which will be further referred to as the standard procedure, to 0.6 wt%. The stock solution was stored at 7°C to prevent ammonia loss by evaporation, and the dilutions were made immediately prior to use.

3.3 Characterization

3.3.1 Transmission Electron Microscopy

Both the shape and average size of the NCs were characterized with Transmission Electron Microscopy (TEM), prior to and after coating with silica. Samples for analysis were obtained by drop casting the NPs solution onto polymer-coated copper TEM grids at room temperature. Solutions of silica-coated NCs in ethanol were first sonicated (5 min.) in order to prevent agglomeration on the grid. The TEM images presented in this chapter were obtained with a Tecnai12 microscope operated at 120 kV and equipped with a tungsten filament. Images were recorded with a SIS Megaview *II* CCD-camera in iTEM software. STEM images were acquired on an FEI Tecnai20FEG instrument equipped with a Fischione HAADF-detector operated at 200 kV acceleration voltage. Energy Dispersive X-ray Spectroscopy (EDS) spectra were acquired with an EDAX detector using Tecnai Imaging and Analysis software (TIA). The cryo-TEM measurements were performed on a diluted solution of CdSe NPLs (200 µL of the stock solution in hexane was added to 10 mL cyclohexane) drop casted on a TEM grid and instantly frozen with liquid nitrogen. These were measured on a FEI Tecnai20FEG operating at 200 kV using a Gatan 914 Nitrogen cooled Cryotransfer Tomography holder.

3.3.2 Optical spectroscopy

The NR concentration was estimated using inductively coupled plasma atomic emission spectroscopy (ICP-AES), in combination with absorption spectroscopy. The concentration of NPLs is indicated by the optical density (OD) at 400 nm. Samples for optical analysis were prepared by diluted of the stock

solution in a quartz cuvette. Absorption spectra were measured on a Perkin-Elmer Lambda 950 UV/VIS/IR spectrometer. The emission spectra were recorded using an Edinburgh Instrument FLS920 with a 450 W Xenon Lamp as the excitation source. An excitation wavelength of 450 nm was used for the NRs, whereas an excitation wavelength of 380 nm was used for the NPLs.

3.4 Results and discussion

3.4.1 Silica coating of CdSe/CdS core/shell NRs and varying the ammonia concentration

NRs coated with silica according to the standard procedure
CdSe/CdS core/shell NRs were synthesized by the seeded growth method as described in paragraphs 3.2.2 and 3.2.3. Figure 3.1 shows TEM images of NRs of different sizes, experimental details of the synthesis of these samples are summarized in Appendix A and B.
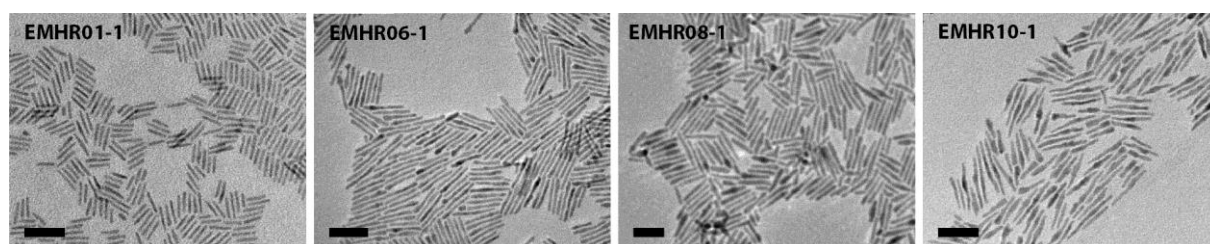

Figure 3.1: TEM overview of CdSe/CdS core/shell NRs of different sizes, from left to right: 23.5 ± 2.7 nm by 4.3 ± 0.6 nm (EMHR01-1), 45.5 ± 4.2 nm by 4.6 ± 0.6 nm (EMHR06-1), 48.5 ± 6.3 nm by 6.2 ± 0.9 nm (EMHR08-1) and 50.9 ± 14.5 nm by 5.2 ± 1.1 nm (EMHR10-1). Experimental details can be found in Appendix A and B. All scale bars correspond to 50 nm.

This type of NRs was recently successfully incorporated in silica with the reverse microemulsion method by Pietra *et al.*[72] The difference in both conformation and crystallography of the opposite tips allowed for a detailed study on the silica growth mechanism on these anisotropic NCs. As elucidated in paragraph 2.1.3, this type of NR has a pencil-shaped structure with the CdSe core located close to the flat end. Under the usual microemulsion conditions (i.e. the standard procedure with 29.9 wt% ammonia), a silica sphere is formed on the Cd-terminated side of the NR, followed by a smaller one on the other tip leading to dumbbell-type structures. Most likely, the ligand exchange of the original capping ligand ODPA for the silica precursor TEOS is most favorable at these crystallographic facets, which explains the observation that the silica growth starts at the two opposite tips.
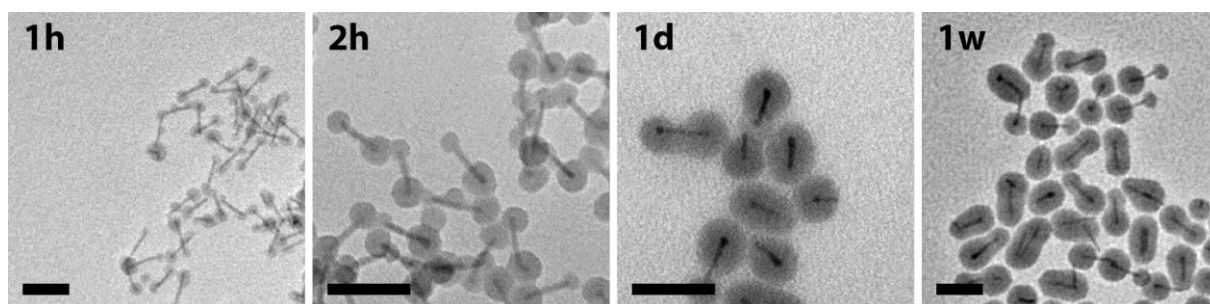
Figure 3.2: Transmission Electron Microscopy (TEM) images of NRs of 37.1 ± 4.1 nm by 4.3 ± 0.3 nm, partially or fully coated with silica by the reverse microemulsion method. Quenched after A) one hour, B) two hours, C) 24 hours and D) one week. All scale bars correspond to 50 nm.

After further growth these silica spheres fuse until the NR is fully incorporated in the shell. This is visualized in Figure 3.2, which shows CdSe/CdS core/shell NRs of 37.1 ± 4.1 nm by 4.3 ± 0.3 nm (130110.2, synthesized by Francesca Pietra, 1.6 nmol) coated with silica at several stages of the

incorporation process. The asymmetric growth at the different tips of the NRs in the early stages is clearly visible after 2 hours, when the silica spheres on the flat Cd-terminated ends have an average radius of 8.8 ± 1.0 nm while the radius of the spheres on the opposite tip is only 5.3 ± 1.1 nm. After further growth, these silica spheres unify to fully cover individual NRs resulting in ellipsoid-shaped NPs (1 day and 1 week). Some remain dumbbell-shaped as their final morphology. Naturally, the growth time and the amount of TEOS required to completely cover the NRs depend on their length.[72] It is clearly visible that under these conditions, every NP contains a single NR. If the concentration of NRs is increased, each silica shell encapsulates more than one NR (see Figure 3.3). On the other hand, decreasing the concentration of NRs leads to empty silica NPs. These findings are consistent with studies on the silica coating of QDs, for which spontaneously nucleated silica NPs were observed for reverse microemulsions in which the concentration of QDs was too low and vice versa.[68,70] These observations can be understood considering that every NR is surrounded by a fixed number of surfactant molecules. If the concentration of NRs is decreased there will be 'free' surfactant molecules that form empty micelles in which silica nucleation and growth take place. On the contrary, if the concentration of NRs is too high, not every NR can be individually surrounded by enough surfactant molecules. Hence, multiple NRs are incorporated in one silica shell.

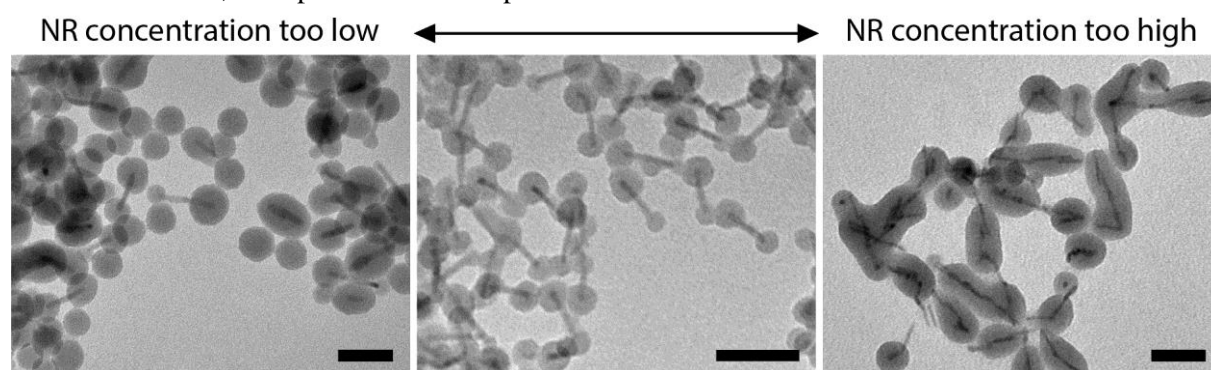NR concentration too low ⟷ NR concentration too high

Figure 3.3: Transmission Electron Microscopy (TEM) images of silica-coated NRs at different concentrations of NRs in the reverse microemulsion. The middle image shows the NPs from Figure 3.2 (2 hours), for which 1.6 nmol NRs was added to the microemulsion. If the amount of NRs is too low (« 1 nmol) empty silica spheres are formed, while at too high NR concentrations (» 2 nmol) multiple NRs are encapsulated in one silica shell. This is displayed in respectively the left and right image. All scale bars correspond to 50 nm.

Influence of the ammonia concentration on the silica shell growth

The CdSe/CdS core/shell NRs from the previous paragraphs were used as a case study to examine the role of the ammonia concentration on the resulting silica shell. Therefore, aqueous ammonia solutions with concentrations varying from 29.9 wt% to 0.6 wt% were used while other parameters were kept constant, as described in paragraph 3.2.7. In literature, an ammonia solution of 25 to 30 wt% is regularly used for silica coating of NCs with the reverse microemulsion method,[27,54] therefore this will be further referred to as the standard procedure.

The silica growth on NRs of 48.5 ± 6.3 nm by 6.2 ± 0.9 nm (EMHR08-1) was followed in time for several ammonia concentrations, see Figure 3.4. Figure 3.4 A shows the evolution of the silica shell over time for NRs coated according to the standard procedure. The formation of dumbbell-type and ellipsoid-shaped NPs is in good agreement with earlier observations (Figure 3.2). Figure 3.4 B displays the silica shell growth for ammonia concentrations of 8.5 wt% and 5.7 wt%. The resulting particles evolve in a similar way as observed for the standard procedure: first dumbbells with silica spheres at the opposite tips are formed, after which the NRs finally become completely covered with silica.
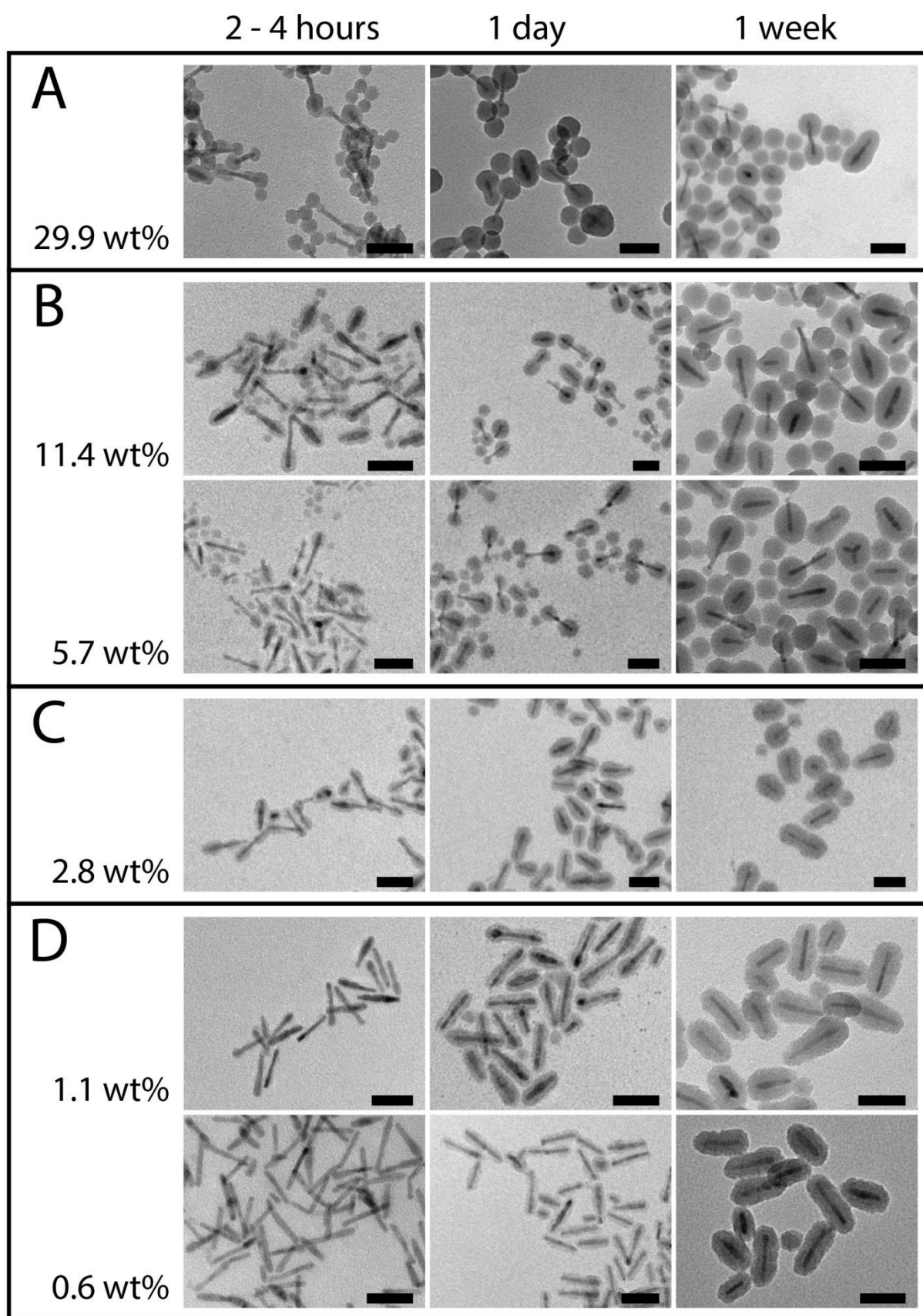
Figure 3.4: TEM overview of silica growth on CdSe/CdS core/shell NRs at different times (x-axis) for several microemulsions equally prepared, but with different ammonia concentrations in the aqueous phase (y-axis). The NPs from A and B were quenched after two hours, one day and one week, while the NPs displayed in C and D have grown for four hours, one day and one week. Modified from Ref. 93.

Also in this regime (i.e. 5.7 to 8.5 wt%), some NRs remain dumbbell-shaped as their final conformation. Therefore, decreasing the ammonia concentration with a factor 5 compared to the standard procedure does not lead to significant variation of the silica shell conformation. On the other hand, a drastic change is observed if the ammonia concentration is decreased to 1.1 or 0.6 wt%, see Figure 3.4 D. Dumbbell-type particles are no longer observed and the NRs are completely coated by a uniform ultrathin silica shell (2-4 nm), which is best visible after one day of growth. Since the silica is distributed equally over the surface of each NR, its final shape preserves the original proportions and hence the aspect ratio is only slightly reduced. Further growth results in a thicker shell with preservation of the original shape. For an ammonia concentration of 2.8 wt%, see Figure 3.4 C, the obtained particles show a conformation intermediate to the dumbbell shape and the rod shape obtained with respectively higher and lower ammonia concentrations. In this case, the silica starts to grow on both ends of the NRs, but appears less spherical and more elongated along the z-axis compared to the characteristic dumbbell-type particles. This is best visible in the early stages (2-4 hours). The effect of the ammonia concentration on the resulting shell thickness was quantified by measuring the temporal evolution of the average shell thickness (Figure 3.5). The thickness was measured at the thickest point, perpendicular to the z-axis of the NR. In the early stages, see blue triangles at 1 and 2 hours, 29.9 wt% ammonia leads to significantly faster growth than the lower concentrations. The growth is nearly complete after one day, since the shell barely increases in size afterwards (the curve reaches a plateau). For 8.5 wt% ammonia, see green stars at 1 and 2 hours, the shell is significantly thinner in the early stages. However, after one day these shells display the same thickness as those from the standard procedure. For an ammonia concentration of 2.8 wt%, see yellow diamonds, the shells remain thinner during the first few days. However, after four to five days (time ≈ 100 hours) the thickness is getting close to the standard procedure.
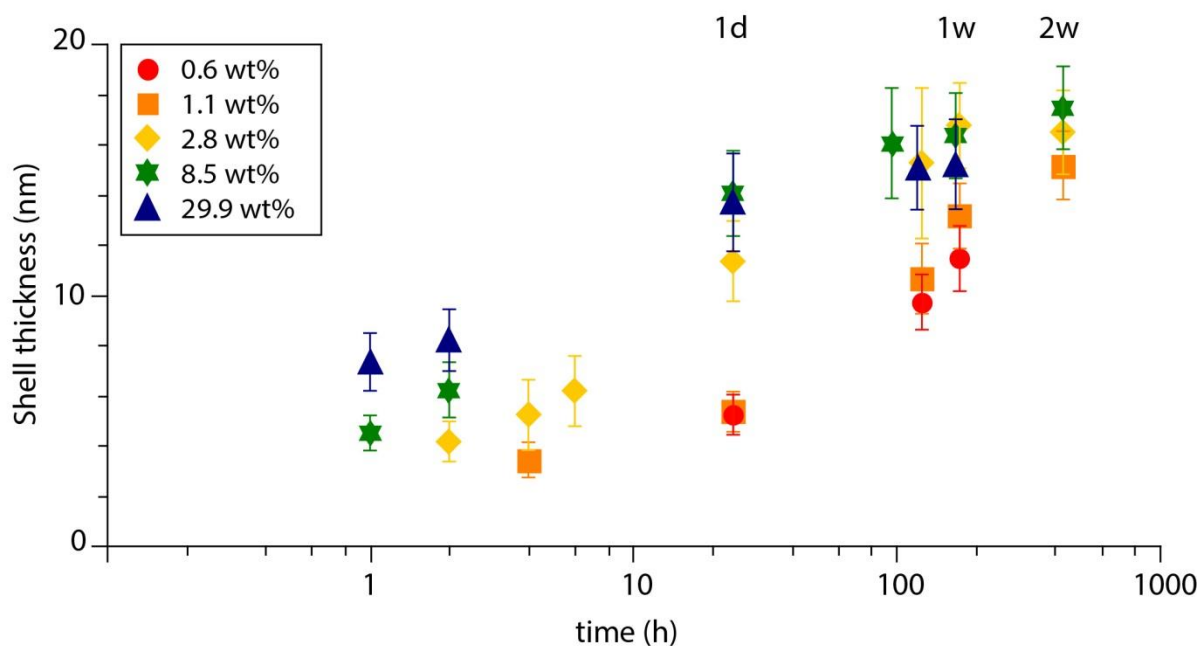
Figure 3.5: Semi-logarithmic plot of the silica shell thickness evolution over time for different concentrations of ammonia. Growth times of one day, one week and two weeks are denoted by 1d, 1w and 2w, respectively. The data points correspond to the samples displayed in Figure 3.4 (except the ones at 2w). Reproduced with permission from Ref. 93.

For concentrations of 1.1 and 0.6 wt% on the other hand, see orange squares and red circles, an ultrathin silica shell of approximately 2 nm was observed on the NRs in the first few hours. However, due to the limited resolution of the TEM the exact thickness of this shell was hard to quantify. With an ammonia concentration of 1.1 wt%, a uniform thin shell of only 3 nm was measured after 4 hours of

growth. After one day, the silica shells of 1.1 and 0.6 wt% display an equal thickness of only 5 nm, which is substantially thinner than the shells of at least 11 nm obtained with higher concentrations. Only after one week of growth these originally ultrathin shells start to approach the dimensions of the dumbbells and after more than two weeks, all the shells display a comparable thickness. This is considered to be the final conformation, as an additional growth time of ten weeks does not significantly change the size and shape of the silica shell (Appendix E). Note that, although the shell thicknesses are (almost) the same for the different ammonia concentrat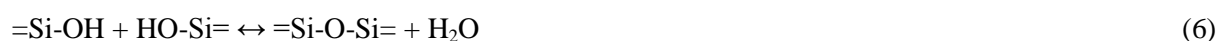ions, the silica volume around the completely incorporated NRs is larger than the silica volume of the dumbbell-type particles.

Importantly, another effect of lowering the ammonia concentration is that the number of self-nucleated silica NPs decreases (see Figure 3.4). Whereas high ammonia concentrations produce a significant number of empty silica spheres (Figure 3.4 A and B), low ammonia concentrations (Figure 3.4 C and D) rarely lead to the self-nucleation of silica NPs. As elucidated before, the degree of self-nucleated silica NPs is highly dependent on the concentration of NCs and is regularly minimized upon increasing the concentration of NCs. Interestingly, the same effect is observed in case of lowering the ammonia concentration (less than 2.8 wt% in this case). Given that the concentration of surfactant molecules and NCs is the same in all microemulsions, the self-nucleation of silica could hence also be reduced by lowering the ammonia concentration.

Proposed mechanism for silica growth with lower ammonia concentration

In literature, high ammonia concentrations are frequently used to obtain spherical silica shells, as low ammonia concentrations yield irregular shapes.[65,68,94,95] In the case of anisotropic NCs, reducing the tendency to grow silica into spheres facilitates the formation of uniform anisotropic shells. In order to understand these observations, the chemical processes involved in the nucleation of silica needs to be considered: hydrolysis and poly-condensation of TEOS monomers. The first step is the hydrolysis of one to four (x) ethoxy groups of individual TEOS monomers:

$$\text{Si(OC}_2\text{H}_5)_4 + x\text{H}_2\text{O} \leftrightarrow \text{Si(OC}_2\text{H}_5)_{4-x}(\text{OH})_x + x\text{C}_2\text{H}_5\text{OH} \tag{5}$$
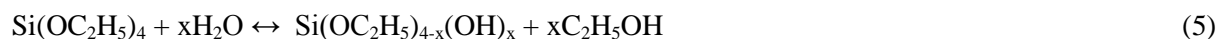
In the second step, hydrolyzed TEOS monomers (poly-)condensate forming covalent bonds, thereby producing water or ethanol. These condensation reactions involve the attack of a nucleophilic (deprotonated) silanol on a neutral species:

$$\equiv\text{Si-OH} + \text{HO-Si}\equiv \leftrightarrow \equiv\text{Si-O-Si}\equiv + \text{H}_2\text{O} \tag{6}$$

$$\equiv\text{Si-OH} + \text{H}_5\text{C}_2\text{O-Si}\equiv \leftrightarrow \equiv\text{Si-O-Si}\equiv + \text{C}_2\text{H}_5\text{OH} \tag{7}$$

This leads to the formation of networks that ultimately result in colloidal particles.[95,96] The results presented in Figure 3.4 show that the silica shell growth on the NRs as well as the presence of self-nucleated silica are highly dependent on the ammonia concentration. Both effects are attributed to a competition between the attachment of TEOS monomers to the NR surface (i.e. ligand exchange) and the poly-condensation into a network. In the microemulsion system, both hydrolysis and condensation steps are base catalyzed by the hydroxide ions from the aqueous ammonia solution. Hence, the ammonia concentration determines the rate of hydrolysis (eq. (5)) and condensation (eqs. (6) and (7)) and therefore affects the balance between the rates of surface attachment and network formation. With 29.9 wt% ammonia, TEOS monomers are quickly completely hydrolyzed. Since these monomers are deprotonated due to the high pH value (pH ~ 10.5, pK$_a$ of silicic acid: 9.8), rapid poly-condensation (eqs. (6) and (7)) leads to fast network formation.[96] In the presence of a NR, hydrolyzed TEOS monomers are attracted towards partly positively charged Cd-atoms on the NR surface and hence replace the original capping molecules, starting at the most reactive facets (i.e. the opposite tips).[72] These two processes (network formation and surface attachment) occur simultaneously.

Consequently, networks are formed both in empty micelles and at the tips of the NRs. After reaching a critical size these grow into silica spheres, leading to the dumbbell-type structures as well as self-nucleated spheres displayed in Figure 3.4 A. For ammonia concentrations down to 5.7 wt% (pH > 9.8) the same growth behavior is observed, i.e. dumbbell-formation and self-nucleation (Figure 3.4 B). However, the hydrolysis and poly-condensation are obviously slower, since a thinner shell is observed in the early stages (Figure 3.5). Nevertheless, as long as the TEOS monomers each have at least two hydrolyzed groups, the poly-condensation into networks will be faster than TEOS attachment to the entire surface of the NRs. With less than 2.8 wt% ammonia, the hydrolysis is much slower and therefore TEOS monomers will be only partly hydrolyzed. In this case, the hydrolysis is a rate-limiting step for the poly-condensation into networks, because condensation upon removal of an ethoxy group is less favorable than removal of a hydroxyl group (due to steric factors). Consequently, the attachment of hydrolyzed TEOS monomers to cadmium atoms on the NR surface becomes faster than the network formation. In this regime, the original capping ligands are probably completely exchanged for TEOS monomers before stable networks are formed in solution. Poly-condensation between TEOS monomers attached to the NRs finally leads to networks at the entire surface of individual NRs. Hence, a uniform silica shell is formed around the entire NR instead of silica spheres at the opposite tips and in empty micelles. The two extreme situations are represented schematically in Figure 3.6.
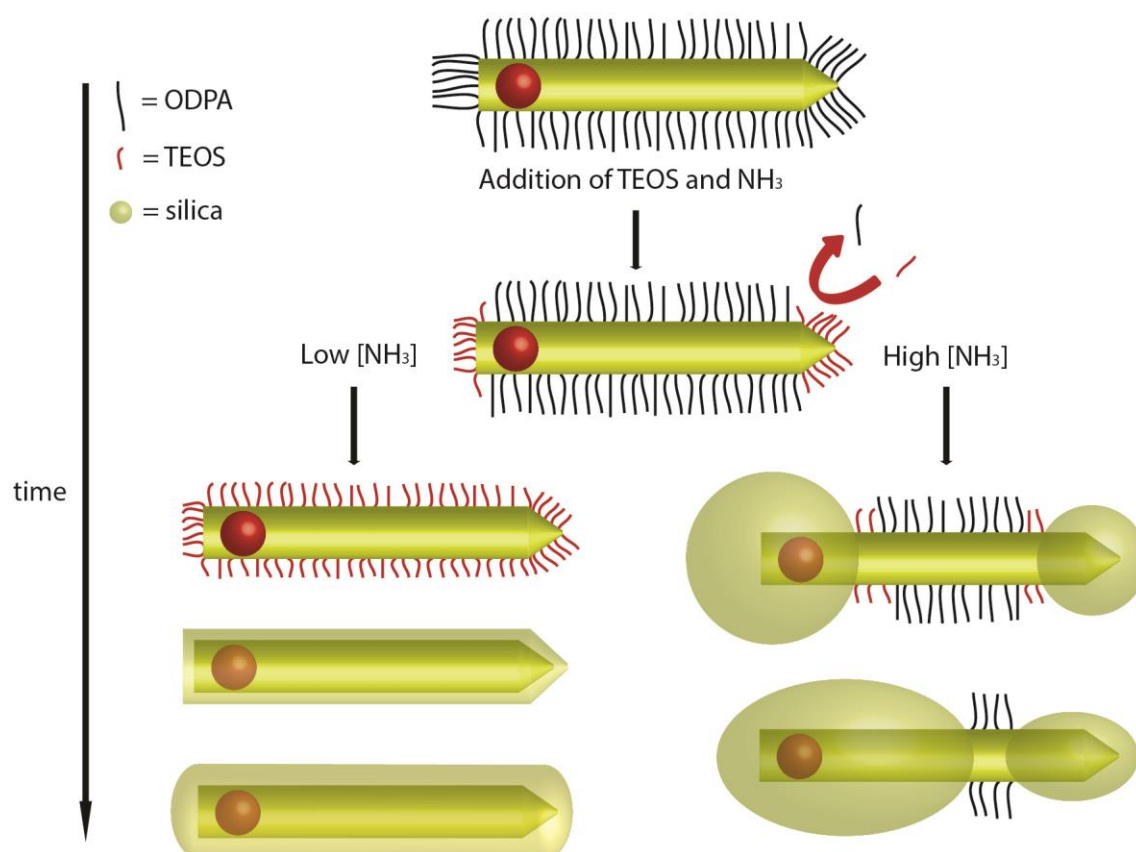
Figure 3.6: Schematic representation of the silica growth on CdSe/CdS core/shell NRs under a low (left) and high (right) ammonia concentration. In both cases, the ligand exchange of ODPA for (hydrolyzed) TEOS starts at the most reactive facets, indicated by the red arrow. If the concentration of ammonia is high, this is rapidly followed by growth of silica spheres at the opposite tips. At sufficiently low ammonia concentrations, the ligands are completely exchanged before a uniform silica shell is formed at the entire surface of the NRs. Naturally, there is a gradual transition from the dumbbell- to the rod-type particles as the concentration of ammonia varies between the two extremes. Reproduced with permission from Ref. 93.

As mentioned before, the volume of the silica shell around completely incorporated NRs is larger than that of dumbbell-type particles (considering the shells are of equal thickness). Assuming that these shells have the same density, this suggests that at the final stage (Figure 3.5, 2 weeks) more TEOS monomers have been consumed by the shells around the fully coated NRs than the shells around the dumbbells, which are accompanied by empty silica spheres. This could be explained considering that TEOS monomers can be exchanged between micelles upon collision.[69] This is attributed to the hydrophobicity of the TEOS monomers, which depends on the ammonia concentration. If hydrolysis is incomplete due to a low ammonia concentration, the partially hydrolyzed TEOS monomers are relatively hydrophobic and therefore expected to reside at the surfactant layer of the micelles.[69] Upon collision of two micelles, these TEOS monomers can migrate from an empty micelle to a micelle containing a NR and hence contribute to the silica shell around the NR. On the contrary, with high ammonia concentrations the TEOS monomers will be rapidly hydrolyzed, become hydrophilic and consequently move from the surfactant layer into the micelles followed by condensation into networks. Hence, these will not be exchanged upon micelle collision. This explains the observation that for the higher ammonia concentrations all the precursor is depleted before the silica spheres at the tips of NRs unify, while for the lower ammonia regimes there is enough TEOS precursor available for the silica shells to keep growing (Figure 3.5). Note that, the formation of silica NPs could also occur in the lower ammonia regime, however the minimum NC concentration required to prevent self-nucleation is lower.

During this work, the formation of a uniform silica shell on anisotropic NCs with the reverse microemulsion method was reported for CdSe/CdS core/shell tetrapods.[75] Contrary to the explanation given above, the authors ascribe this to relatively *fast* hydrolysis and condensation resulting from the addition of extra water which increases the water-to-surfactant ratio. However, if water is included to the ammonia solution prior to addition to the microemulsion this is in fact similar to dilution of the ammonia solution. To exclude that the uniform silica shell around the NRs might be due to an increase of the water-to-surfactant ratio, these were coated with silica in a microemulsion with half the amount of aqueous solution. The concentration of ammonia in this solution was 1.5 wt% and all other parameters were kept constant. Figure 3.7 displays that this also yielded uniform silica shells, instead of silica spheres at the opposite tips. The latter would be expected if the thin layer was resulting from extra water. Hence, it can be concluded that a low ammonia concentration plays a major role in the formation of a uniform silica shell and that this is independent of the water-to-surfactant ratio.
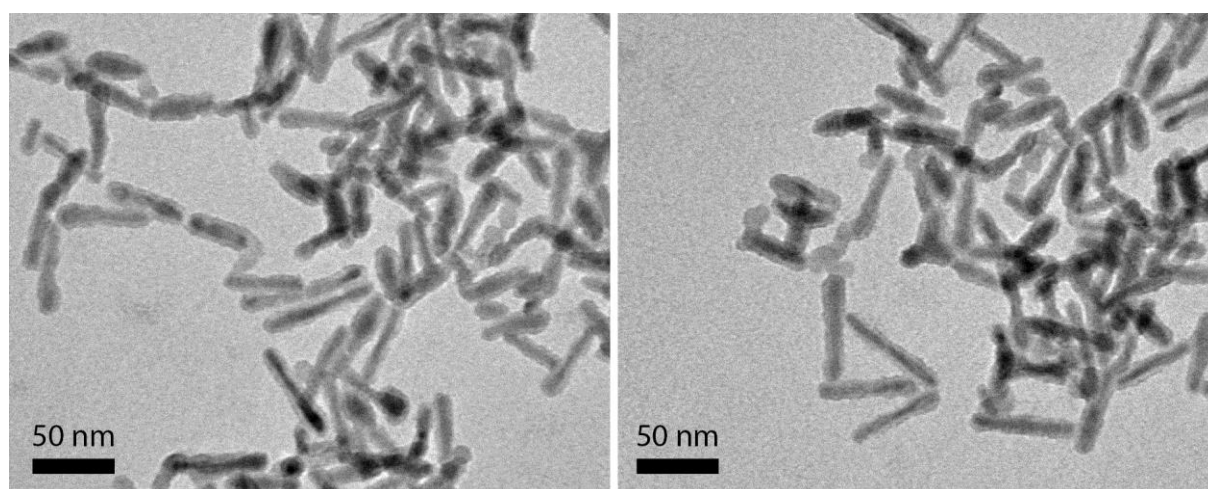

Figure 3.7: TEM images of NRs isolated after 24 hours from a microemulsion with 1.5 wt% ammonia in the aqueous phase. In this case, 75 μL ammonia solution was added instead of 150 μL, while all other parameters were kept constant. Reproduced with permission from Ref. 93.
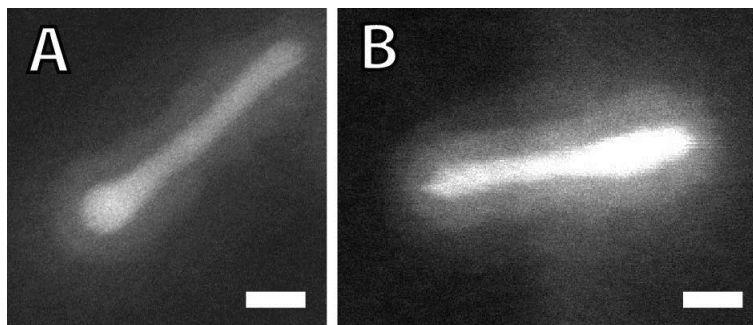
Figure 3.8: HAADF-STEM images of CdSe/CdS core/shell NRs coated with silica in a microemulsion with 1.5 wt% ammonia. Experimental details are in Appendix C. Scale bars correspond to 10 nm.

To further support the proposed model, HAADF-STEM analysis combined with EDS (Appendix F to H) was performed. HAADF-STEM images (Figure 3.8) of individual NRs coated with silica in a microemulsion with 1.5 wt% ammonia clearly show that the uniform silica shell not only adapts to the rod-shape, but also to the bulb originating from the CdSe core embedded in the CdS rod. Hence, these conditions ensure preservation of the original shape anisotropy. Appendix F shows an image and corresponding EDS analysis on NRs isolated from a microemulsion with 1.1 wt% ammonia after two hours of growth. Although no silica layer could be observed, EDS analysis on a group of these particles confirmed the presence of silicon (Si) and phosphor (P) at the NRs. Thus, at this stage both TEOS monomers and the original capping ligand ODPA are on the surface, which means that the ligand exchange is in progress. NRs isolated after one day from a microemulsion with 1.5 wt% are completely coated with silica, as shown in Figure 3.8. EDS analysis on these particles confirmed that at this stage, ODPA is completely removed (Appendix G), as phosphor is no longer present. On the contrary, phosphor could be detected on NRs isolated after one day from a microemulsion with 29.9 wt%, see Appendix H. This gives evidence to the idea that with a low ammonia concentration (1.5 wt%) the original capping ligand is completely exchanged, whereas with the high ammonia concentration (29.9 wt%) the ligand exchange is only partial with the same growth time of one day.

Optical properties of silica-coated CdSe/CdS core/shell NRs

As mentioned before (2.1.4), a major advantage of the incorporation of semiconductor NCs in silica is the preservation of optical properties in water- and oxygen-rich environments. It was shown that CdSe/CdS core/shell NRs coated with silica according to the standard procedure remained highly luminescent for at least two weeks upon constant exposure to oxygen, especially if these were stored in a nonpolar solvent (i.e. toluene).[72] Whether the ammonia concentration during the silica coating procedure affects the optical properties of the NRs has not yet been reported. In this paragraph, preliminary results are shown on the comparison of NRs coated with silica according to the standard procedure to NRs coated in presence of 1.5 wt% ammonia. Both were quenched after one week of growth. Figure 3.9 A shows that NRs silica-coated with 29.9 wt% ammonia (EMHS53-2, left cuvette) as well as 1.5 wt% ammonia (EMHS54-2, right cuvette) are luminescent under illumination with blue ultraviolet (UV) light.

For both samples, the normalized emission intensity (i.e. the number of emitted photons relative to the number of absorbed photons at the excitation wavelength, see 3.3.2) is shown in Figure 3.9 B. The peaks are at the same emission wavelength of 624 nm, which is slightly shifted compared to the emission at 622 nm for the uncoated NRs (see Appendix I). This might be due to the different environment, as the silica-coated NRs were measured in ethanol while the uncoated NRs were dispersed in toluene. The emission peaks have a full width at half maximum (fwhm) of 54 nm for the standard procedure and 43 nm for the low ammonia concentration, compared to a fwhm of 42 nm for

the uncoated NRs. Thus, the emission peak of the dumbbell-shaped NRs (standard procedure) is broader than the peaks of the uncoated NRs and the completely incorporated NRs and furthermore it is asymmetrical in shape. This could be explained in terms of an inhomogeneity in the environment, i.e. the uncoated parts of the dumbbells are exposed to ethanol whereas the coated tips are surrounded by silica.

Another observation is that the NRs coated with the standard procedure show more effective radiative recombination than the NRs coated with the low ammonia procedure, indicated by the larger peak area. In general, the emission can decrease in efficiency due to surface defects arising during ligand exchange, which is an essential step in the silica coating procedure.[97,98] A possible explanation for the observed difference (Figure 3.9 B) would be that the surface of the dumbbell-type NRs is overall less affected than the surface of the completely coated NRs. According to the proposed mechanism (Figure 3.6) a complete ligand exchange has occurred on the NRs exposed to the low ammonia concentration, which makes the surface of these NRs prone to defects. On the contrary, the middle part of the dumbbells (high ammonia concentration) is expected to remain largely intact with the original capping ligand. Furthermore, it might be that some of the capping ligands remained attached to the NRs also underneath the silica shell if the rate of silica growth is faster than the rate of ligand exchange, inducing less defects. Consequently, the NRs with completely exchanged ligands (low ammonia concentration) are likely to display less efficient radiative recombination than the NRs with only partially exchanged ligands (high ammonia concentration). Although these results suggest that the PL intensity is somewhat better preserved with the standard procedure, more experiments are required to be conclusive.
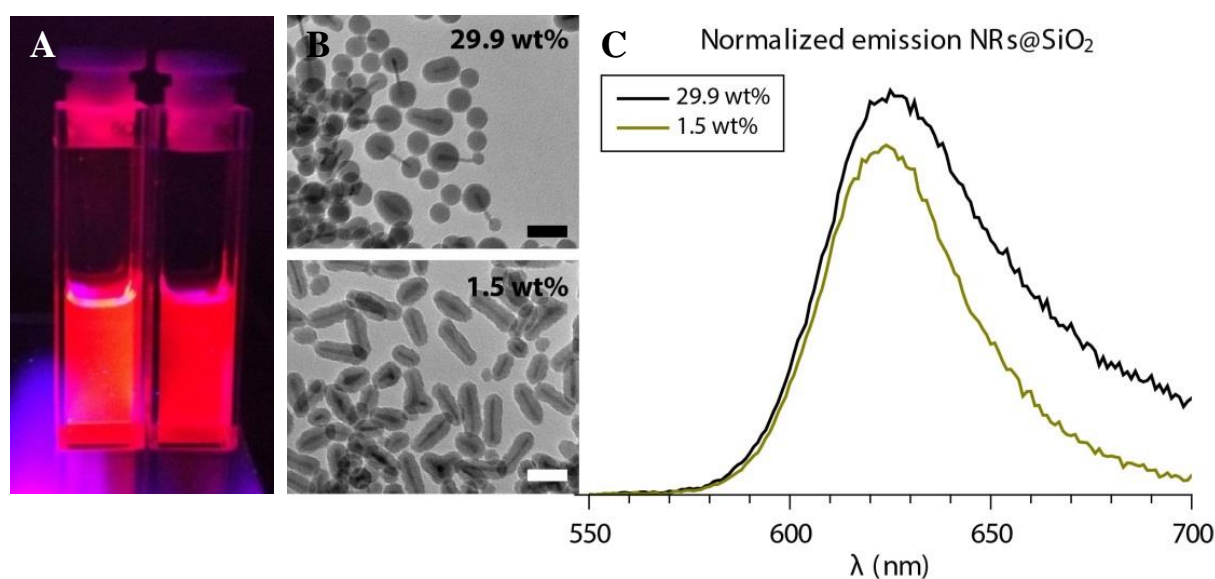

Figure 3.9: A) Diluted dispersions of silica-coated NRs in ethanol, isolated after one week from a microemulsion with 29.9 wt% (left cuvette) and 1.5 wt% (right cuvette), illuminated with blue UV light. Both samples emit red colored visible light. B) TEM images of the samples from (A), scale bars correspond to 50 nm. C) Normalized emission spectra corresponding to the NRs displayed in (A) and (B).

3.4.2   Silica coating of gold-tipped CdSe/CdS core/shell NRs

As mentioned in 2.1.3, an important electronic feature of CdSe/CdS core/shell NRs is that the hole is confined in the core whereas the electron is delocalized throughout the NR. If metal NPs, i.e. platinum or gold, are grown onto the surface of these core/shell NRs, the delocalized electrons are transferred to the metal while the hole remains localized in the core.[47,99] Several methods have been developed to selectively grow platinum or gold on one of the tips of the NRs, after which the electron is physically separated from the hole.[47,99,100] These structures provide high potential for photocatalytic applications,

due to the separation between the oxidizing holes (in the cores) and the hydrogen production sites (in the metal tips). It was found for platinum-tipped NRs that the activity of hydrogen production from water increases with the distance between electron and hole.[47] Therefore, it would be interesting to assemble relatively long (≥ 70 nm) metal-tipped NRs into membranes with their metal tips (i.e. catalytic site) oriented into the same direction. In this respect, it is desirable to make the NRs water-soluble and furthermore protect them towards photodegradation by selectively incorporate them in silica while the catalytic site remains accessible. Preservation of the original shape is required to enable self-assembly into membranes.

In this paragraph, CdSe/CdS core/shell NRs of 137 ± 7.4 nm by 5.7 ± 0.6 nm with a gold tip at the flat terminated end (see 3.2.4 for experimental details) are coated with silica in a microemulsion with 1.5 wt% ammonia. Figure 3.10 shows the resulting silica-coated gold-tipped NRs after 2, 5 and 24 hours of growth.
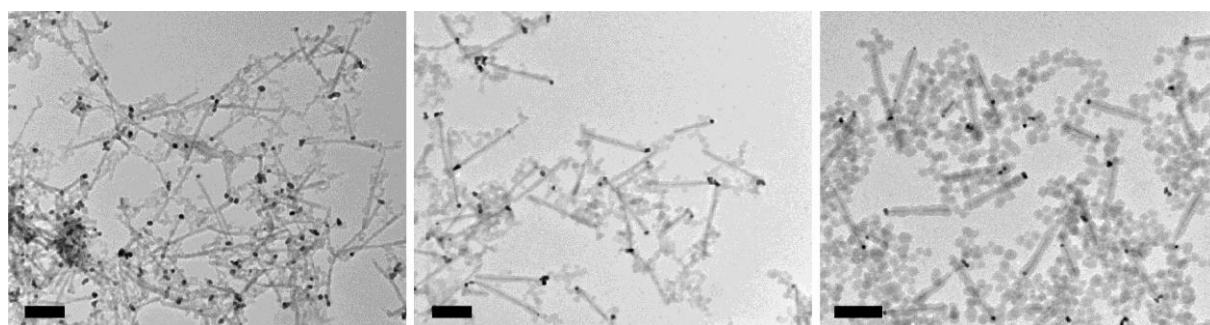

Figure 3.10: CdSe/CdS core/shell NRs of 137 ± 7.4 nm by 5.7 ± 0.6 nm, coated with silica in a microemulsion with 1.5 wt% ammonia, quenched after 2 hours (left), 5 hours (middle) and 24 hours (right).

As predicted in the previous paragraphs, under these conditions the NRs are directly covered with a thin uniform silica shell (less than 3 nm after 2 hours) that thickens by further growth (to 6.4 ± 0.9 nm after 5 hours). Hence, both the high aspect ratio and the shape anisotropy are preserved. Furthermore, no silica has grown on the gold tip, which is stabilized by the organic capping ligand dodecylamine. A plausible explanation for the selective silica growth on the NRs is that the ligand on the gold tip has a substantially higher binding energy than the ligand on the CdS NR. Consequently, the ligand on the gold tip is less easily exchanged for TEOS and hence the hydrolyzed TEOS primarily attaches to the NR surface. This results in silica-coated NRs with a silica-free and thus accessible gold tip. These results not only show the strength of the low ammonia approach to obtain uniform silica shells on highly anisotropic semiconductor NCs, but also provide a versatile method to design NCs that are suitable for photocatalysis.

3.4.3   Silica coating of CdSe NPLs

The CdSe NPLs used in this paragraph, synthesized according to the first protocol from Ithurria *et al.*[37] (see section 3.2.5 for details), are displayed together with absorption and emission spectra in Figure 3.11. The well-defined absorption and emission peaks confirm that the NPLs consist of five CdSe monolayers, which corresponds to a thickness of 1.52 nm.[101] This is very thin compared to the lateral dimensions of 27.9 ± 6.5 nm by 80-140 nm and hence these NPLs are believed to be flexible in solution. [23,37,102] However, their exact morphology is not trivial, since TEM analysis after drying is in this case not representative enough to be conclusive.

Figure 3.12 shows CdSe NPLs coated with silica in a microemulsion with 29.9 wt% (A), 3.0 wt% (B) and 1.5 wt% (C) ammonia in the aqueous phase, quenched at different stages of growth. After three hours of growth, a visible shell of 10-11 nm is formed around the NPLs coated with the standard procedure (i.e. 29.9 wt% ammonia, Figure 3.12 A).
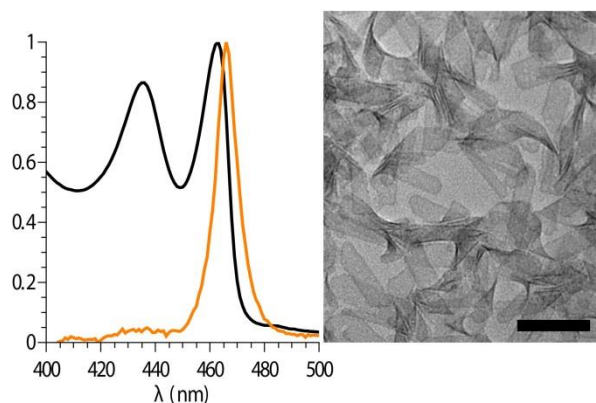
Figure 3.11: Absorption (black line) and emission (orange line) spectra (a.u.) with corresponding TEM image of five monolayer thick CdSe NPLs. Scale bar corresponds to 100 nm.
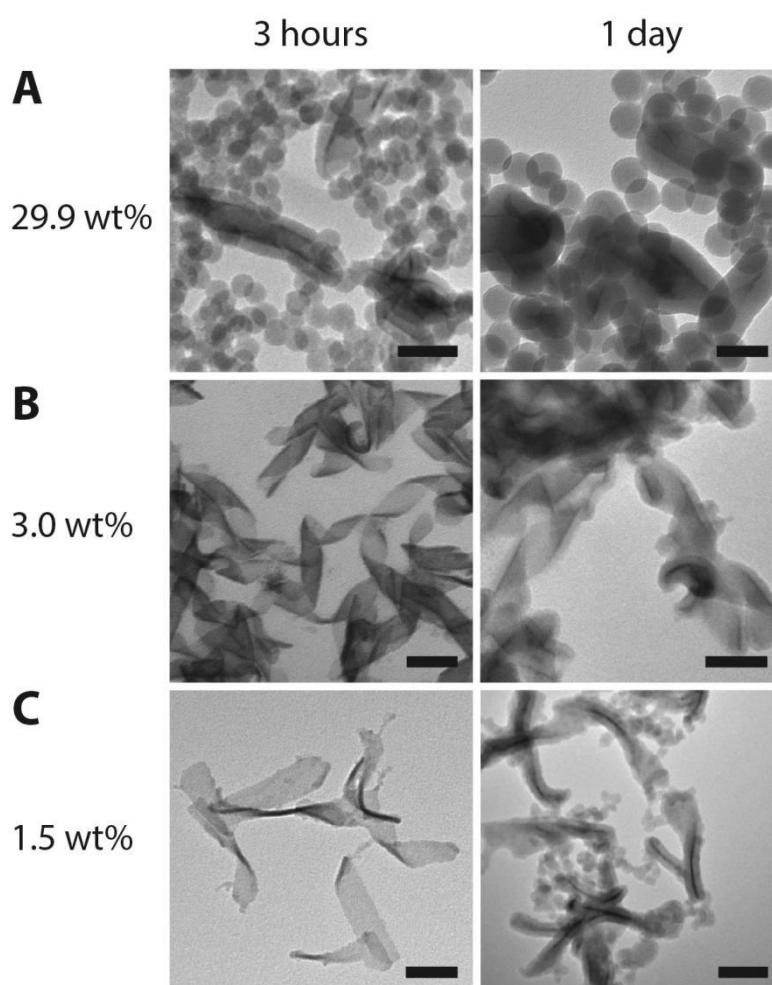
Figure 3.12: TEM overview of CdSe NPLs coated with silica in a microemulsion with 29.9 wt% (A), 3.0 wt% (B) and 1.5 wt% (C) ammonia, quenched at different stages of growth. Scale bars correspond to 50 nm.

If the concentration of ammonia in the aqueous phase is substantially lowered, see Figure 3.12 B and C, the resulting silica shells are much thinner in this early stage (less than 2 nm). After one day, these are 7-9 nm in thickness, while the silica shells around the NPLs coated with the standard procedure are already up to 20 nm at this point. Thus, the ammonia concentration has a significant effect on the thickness of the silica shell around the NPLs, which is in agreement with the observations for the NRs (3.4.1). Considering the crystallographic structure of these NPLs suggested by Dubertret *et al.*,[36,103] the

two opposite main facets are Cd-terminated. The presence of a silica shell on both these main facets is in good agreement with the proposed crystallographic structure, because the hydrolyzed TEOS molecules easily attach to the Cd atoms. Another remarkable difference between the different ammonia concentrations is the morphology of the NPLs encapsulated in silica. The NPLs coated with silica in a microemulsion containing 1.5 wt% ammonia are oriented flat and are individually incorporated in a thin uniform silica shell (Figure 3.12 C). However, for the standard procedure the NPLs appear as rolls inside tubular-shaped silica shells and in some cases multiple NPLs are incorporated within one covering silica shell (Figure 3.12 A). The NPLs coated with 3.0 wt% ammonia are in between these two extremes, i.e. these display a rolled morphology and are individually covered with a thin uniform silica shell.

The exact rolling behavior of the NPLs coated with the standard procedure is barely visible due to the limited resolution of the TEM. Therefore, HAADF-STEM measurements were performed on silica-coated NPLs after one day of growth in a microemulsion with 29.9 wt% ammonia in the aqueous phase, see Figure 3.13. These measurements clearly visualize that the encapsulated NPLs are rolled into a helix-shaped morphology. An ammonia concentration of 3.0 wt% also leads to the incorporation of helices, as shown in Figure 3.12 B. These observations demonstrate that the CdSe NPLs are indeed flexible enough to be either in a rolled or flat morphology.
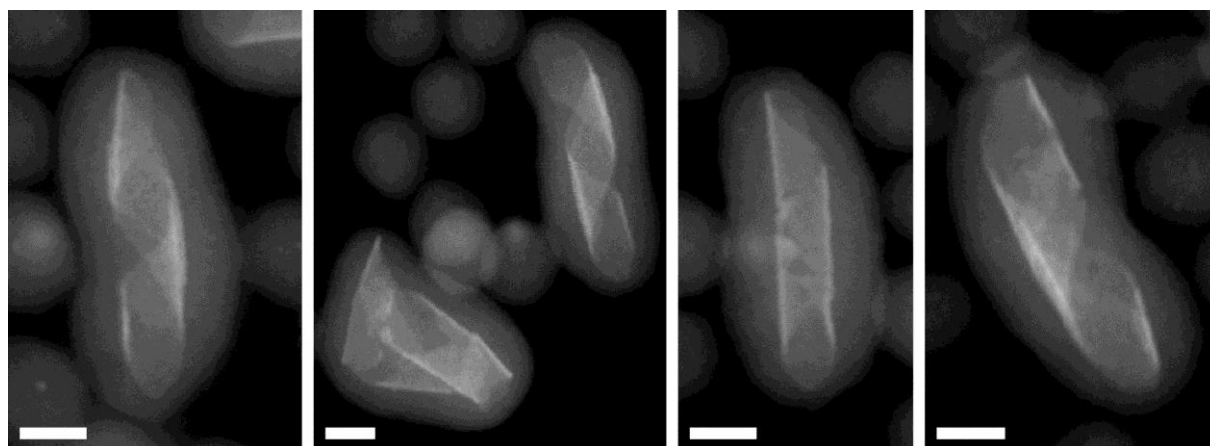

Figure 3.13: STEM-HAADF overview of individual helix-shaped CdSe NPLs coated with silica in a microemulsion with 29.9 wt% ammonia, quenched after one day of growth. Scale bars correspond to 50 nm.

To study the natural appearance of the NPLs in a nonpolar solvent, cryoTEM measurements were performed (3.3.1). A solution comparable to the continuous phase of the reverse microemulsion, i.e. the starting conditions for the silica coating procedure, was quickly frozen on a TEM grid in liquid nitrogen. Figure 3.14 shows a group of CdSe NPLs observed from different angles. Under these conditions, the uncoated NPLs display a helix structure similar to the one observed for the silica-coated NPLs. Consequently, it can be concluded that the helix morphology of the NPLs encapsulated by silica (Figure 3.13 and 3.12 B) is the natural appearance of these NPLs in a nonpolar solvent.

An explanation for the rolling of 2D NCs in solution is a reduction of the high energy coming with the relatively large surface exposed to the direct environment: after rolling only one facet is exposed to the surroundings. Rolled morphologies have been found for CdSe nanosheets that appeared as scrolls on the TEM grid.[35,39,102,104] The rolling into scrolls is attributed to a strain resulting from a difference in electrostatic charge between the two main facets. Most likely, interactions between the ligands on one of the main facets enable the nanosheets to acquire a rolled morphology, i.e. the nanosheets could be unrolled after the growth of a CdS shell, which requires removal of the original ligand.[23,102]
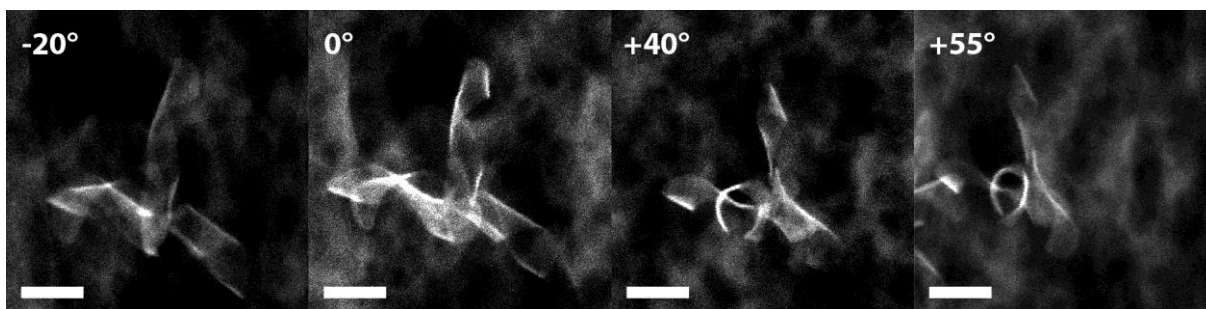
Figure 3.14: cryoTEM images of a group of CdSe NPLs in cyclohexane, viewed from different angles by tilting the TEM grid with respect to the detector. Scale bars correspond to 50 nm.

Considering now that for these CdSe NPLs, the helix structure is the natural appearance in solution, the observations concerning the ammonia-dependent morphology of silica-coated NPLs can be explained with the model proposed in paragraph 3.4.1. That is, a high ammonia concentration leads to silica growth at the crystallographic facets with the highest free energy, whereas a low ammonia concentration yields uniformly coated NCs after a complete ligand exchange.

For a helix-structured NPL, mainly the outer facet is exposed to the solvents and is thus likely to have the highest surface energy. Therefore, with a high ammonia concentration fast silica growth is expected on this facet after which the NPL is unable to unroll. Further growth around the rest of the NPL hence leads to a complete encapsulation of the NPLs in a helix morphology. On the contrary, if the NPLs are incorporated in silica with 1.5 wt% ammonia, a complete ligand exchange occurs prior to the formation of a uniform silica shell. Hence, the ligands are removed from both the outer and the inner facets of the NPLs. Given that the helix morphology is stabilized by interactions between the ligands on the inner facet, the NPLs are likely to unroll when these are exchanged towards TEOS. Therefore, the silica-coated NPLs are in principle unrolled as their final morphology, only slightly bended and twisted. Another observation from the cryoTEM measurements is that some NPLs seem to be attached to each other, see Figure 3.14. More research is needed to reveal if these fused together during (or after) growth or that multiple NPLs originated from a single NC.

Before the silica treatment, the as-synthesized NPLs displayed sharp emission at a wavelength of 466 nm with a fwhm of less than 20 nm. However, there was no PL detected for the silica-coated NPLs, which is explicable considering that the ultrathin NPLs are very sensitive towards changes on the surface. Most likely, the ligand exchange prior to silica growth induced too many defects on the surface of the NPLs, affecting their PL. In spite of the completely quenched emission, the silica-coated NPLs absorbed light of well-defined energies. In Figure 3.15, the absorption spectrum of the uncoated NPLs (black line) is compared to the spectra of the NPLs coated with silica at different ammonia concentrations (colored lines). It is clearly visible that after silica coating, the absorption energies shifted to higher wavelengths (red-shift) and furthermore the curves of the silica-coated NPLs are considerably broader than the sharp peaks of the uncoated NPLs. Both the position and the shape of the absorption curve are dependent on the ammonia concentration and the growth time. These red-shifts started to occur during the coating procedure within a few minutes after addition of ammonia, indicated by the observation that the colors of the microemulsions gradually changed from bright yellow to orange. Red-shifts in the absorption spectra after silica coating have been observed before for gold and semiconductor NCs. However, these are regularly in the order of a few nanometers and can be attributed to the different environment.[27,55,57,64,72,105] For these silica-coated NPLs the red-shift is substantially larger (in the order of tens of nanometers) and hence it is questionable whether it originates only from the silica shell.
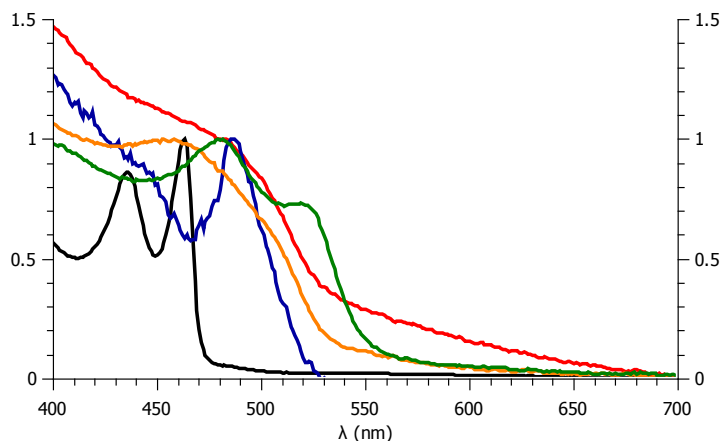
Figure 3.15: Absorption intensity (a.u.) for CdSe NPLs (black), coated with silica in microemulsions with 1.5 wt% ammonia (orange line: 3 h, green line: 24 h), 3.0 wt% ammonia (blue line, 3 h) and 29.9 wt% ammonia (red line, 24 h).

Interestingly, the peak positions of the flat silica-coated NPLs (1.5 wt%, 24 h) correspond to those of six-monolayer thick CdSe NPLs (2.4 and 2.6 eV),[101] which leaves open the possibility of an extra crystalline layer. In this respect, there are two highly speculative scenarios. The first is a surface reconstruction, i.e. interparticle diffusion of atoms that slowly changes the NC shape towards the Gibbs-Curie-Wulff equilibrium shape.[106] The surface atoms are relatively mobile if the original capping ligand is removed but not yet replaced by TEOS. Hence, a surface reconstruction becomes more likely as the rate of hydrolysis of TEOS is slow relative to the rate of ligand exchange. This explains that the red-shift depends on both the ammonia concentration and the growth time.

Another possibility is that, after a slow and complete ligand exchange, the oxygen atoms of TEOS are positioned as an extra crystalline layer on the NPL surface (like CdO). Consequently, the exciton will be less confined resulting in a red-shift that increases with the extend of ligand exchange (ammonia concentration and time). Whether one of these explanations is plausible could be examined with high resolution TEM, that might visualize an extra atomic layer on silica-coated NPLs.

3.4.4 Silica coating of CdSe/CdS core/shell NPLs

The CdSe NPLs from paragraph 3.4.3 were coated with a CdS monolayer, as described in the experimental section. The monolayer was grown with the layer-by-layer growth, in which the original capping ligand (i.e. oleic acid) is first replaced by a sulfur layer originating from bis(trimethylsilyl) sulfide. Then, an extra cadmium layer is grown after addition of cadmium oleate and the core-shell NPLs are once again stabilized by oleic acid. These NPLs, less than 2 nm in thickness and 27.6 ± 8.3 nm by 123.6 ± 24.3 nm in their lateral dimensions, were incorporated in silica with the reverse microemulsion method. An ammonia concentration of 1.5 wt% was used to promote thin shell formation and a standard synthesis using 29.9 wt% ammonia was carried out for comparison. Figure 3.16 shows TEM images of 2D CdSe/CdS NPLs before (Figure 3.16 A) and after silica coating (Figure 3.16 B and C) in a microemulsion with 1.5 wt% ammonia. The shell thickness varies from 3-4 nm after 3 hours of growth to more than 10 nm after one day. After silica coating, most of the NPLs are upstanding and hence observed from the lateral side. Furthermore, the NPLs are slightly bended and twisted after incorporation in silica. To confirm that the high intensity lines are upstanding NPLs, single particles were imaged from different angles by tilting the TEM grid with respect to the detector (Figure 3.16 D). This shows that, comparable to the observations for the NRs and CdSe NPLs, all facets are covered with silica.
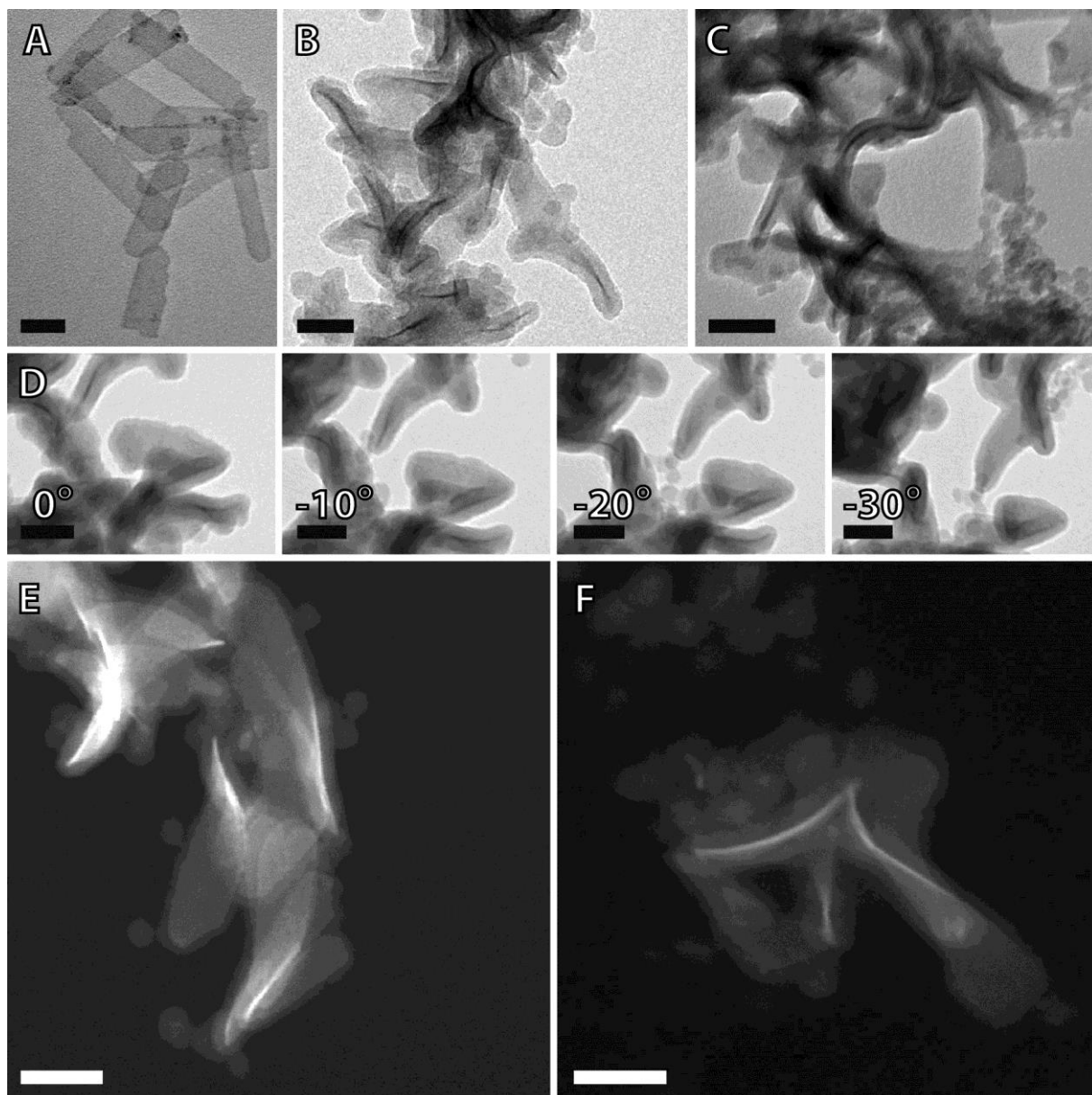
Figure 3.16: TEM images of (A) CdSe/CdS core/shell NPLs and (B,C) silica-coated NPLs with 1.5 wt% ammonia after one day and (D) single silica-coated NPLs considered from different angles. (E,F) HAADF-STEM images of silica-coated NPLs. All scale bars correspond to 50 nm. Reproduced with permission from Ref. 93.

Additionally, HAADF-STEM images show that the shape of the silica shell perfectly adapts to the original proportions of the NPLs (see Figure 3.16 E and F). EDS analysis on these NPLs confirm the presence of Cd, Se, S and Si (see Appendix J). This suggests that the CdS monolayer was successfully formed around the CdSe NPL and besides remained intact during the silica treatment, although a reconstruction of surface atoms cannot be not excluded.

The experiment was repeated with 29.9 wt% ammonia, which also led to the incorporation of NPLs in silica (see Figure 3.17). For this high ammonia concentration, the final morphology of the encapsulated NPLs is twisted and bended as well. Furthermore, the silica shells grew significantly faster and there is relatively more self-nucleation of silica spheres. However, the difference in final shape between the high and low ammonia concentrations is apparently not as drastic as for the NRs and the CdSe NPL helices from the previous paragraphs.

Figure 3.17: TEM images of CdSe/CdS core/shell NPLs coated with silica in a reverse microemulsion with 29.9 wt% ammonia in the aqueous phase, quenched after 3 hours. The silica sh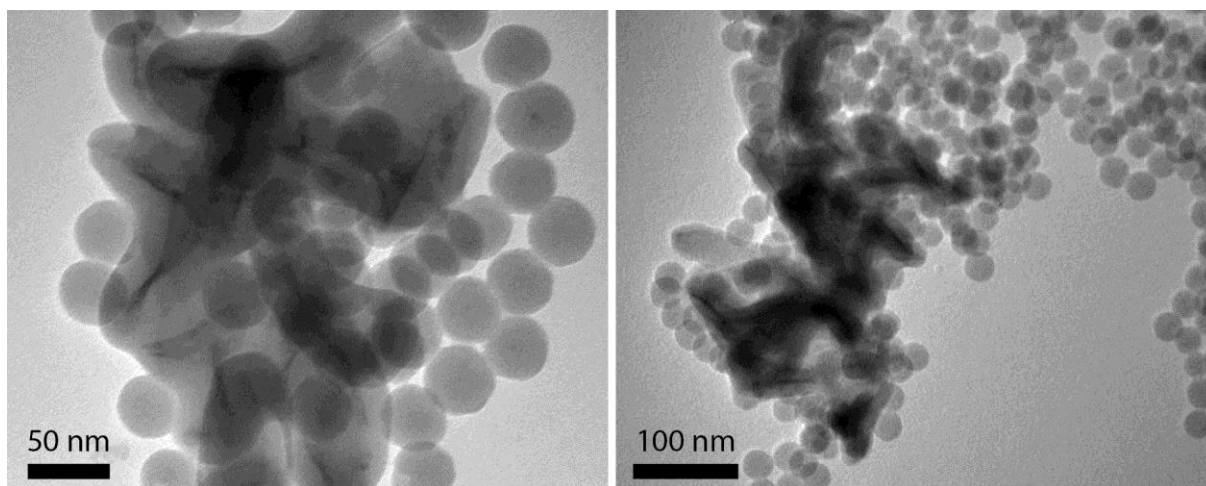ell is clearly less uniform and much thicker than for 1.5 wt% ammonia and there is a huge number of self-nucleated silica spheres.   Reproduced with permission from Ref. 93.

It is highly likely that the bends and twists observed for the core-shell NPLs result from incomplete flattening of the CdSe helix, that occurred during the growth of the CdS shell as a result from removal of the original ligand. These morphologies are similar to the unrolled helices (Figure 3.12 C) observed for the CdSe NPLs that were slowly incorporated in silica, i.e. for which is supposed that the ligand is completely exchanged to TEOS. Therefore, the bended and twisted conformations observed for these core-shell NPLs support the idea that the helix morphology is stabilized by the ligand.

The NPLs were unfortunately no longer luminescent after the growth of the CdS shell and consequently, the effect of the silica shell on the emission could not be studied for these NPLs. The absorption spectra of these NPLs prior to and after silica coating are presented in Appendix K. For both the high and low ammonia concentrations, the silica-coated NPLs display a red-shift of tens of nanometers. This could be attributed to the different environment, i.e. liquid hexane for uncoated NPLs compared to solid silica for coated NPLs. The silica coating of CdSe/CdS core/shell NPLs could be optimized by using a higher concentration of NPLs in the microemulsion, which prevents self-nucleation of silica. Furthermore, it would be very interesting in terms of applications (e.g. in biological environments or plastic crystals) to design luminescent silica-coated core/shell NPLs.

3.5   Discussion

In the previous paragraphs, it was shown that 1D and 2D anisotropic NCs can be coated with a uniform silica shell with the reverse microemulsion method if the concentration of ammonia is decreased to 0.6-1.5 wt%. In this respect, the following kinetic steps are proposed to be essential: (i) slow hydrolysis of TEOS and (ii) complete exchange of the original ligand for (hydrolyzed) TEOS. In this chapter, the thickness of the shell is controlled by the duration of growth before quenching, starting from thin silica shells of less than 3 nm. The comparison between the anisotropic NCs is qualitative, because the exact growth rates cannot be generalized for different NC types. After all, these depend on the concentration of NCs/TEOS as well as different parameters characteristic for each NC structure such as the surface energy and the rate of ligand exchange. Altogether, the results indicate that this method can be used to incorporate a wide variety of anisotropic NCs in a uniform silica shell that preserves the original shape, provided the native ligands are exchangeable for TEOS. Furthermore, this method provides high control over the thickness of the silica shell as this can be tuned from approximately 3 to 17 nm. It would be interesting to study the limits of this approach, i.e. under which conditions silica shells of only one or two monolayers could be formed.

Further, the results demonstrate that, regardless of the ammonia concentration, NCs that are highly anisotropic and besides relatively large in at least one dimension (up to 150 nm) can be incorporated in silica with the reverse microemulsion method. The model of silica growth on isotropic QDs in the reverse microemulsion assumes spherical aqueous micelles with QDs trapped inside. This reasonably explains the observation that QDs of a few nanometers can be encapsulated in the middle of silica spheres of approximately 30 to 50 nm.[27] However, this classical model of spherical aqueous micelles around individual NCs becomes questionable considering that relatively large anisotropic NCs can be coated with a uniform non-spherical silica shell. It would be interesting to study whether, in these systems, spherical or anisotropic micelles are formed around the NCs or if the role of the surfactant is different than previously proposed. Indeed, the NCs are originally hydrophobic and could hence only be completely transferred into water if their ligand is exchanged for a hydrophilic ligand. In this respect, hydrolyzed TEOS is a compatible candidate. However, in the reverse microemulsion (with a nonpolar continuous phase and surfactant micelles surrounding water) the NCs are expected to be dispersed in the continuous phase and the hydrolyzed TEOS will be inside the aqueous phase. Hence, the proposed model of a direct ligand exchange from ODPA to TEOS might be oversimplified.

3.6   Conclusion

In this chapter, different anisotropic NCs such as 1D NRs and 2D NPLs were successfully coated with silica. It was demonstrated that the final morphology of anisotropic NCs incorporated in silica with the reverse microemulsion method is highly dependent on the concentration of ammonia in the aqueous phase. The prominent role of ammonia was first examined with a case study of CdSe/CdS core/shell NRs and it was found that 0.6 to 1.5 wt% ammonia in the aqueous phase results in thin silica shells that perfectly adapt to the original shape of the NRs. Under these conditions, the thickness of the silica shell was highly tunable from less than 3 nm to 17 nm by varying the time of growth. Similar experiments were performed with ultrathin (five monolayer thick) CdSe NPLs, which resulted in the incorporation of helix-shaped as well as flat unrolled NPLs in silica. A further study of the uncoated NPLs with cryoTEM led to the conclusion that the natural morphology of the CdSe NPLs dispersed in a nonpolar solvent is helix-shaped, which can be *"frozen"* by fast incorporation in silica. Finally, slightly bended 2D CdSe/CdS core/shell NPLs were incorporated in silica under both high and low ammonia concentrations. The silica shell grows obviously faster on the NPLs with a high ammonia concentration, however the final morphologies are not notably different. Comparable to the NRs, the uniform silica shells around the NPLs obtained with 1.5 wt% ammonia were tunable in size from less than 3 nm to 10 nm.

Altogether, the results in this chapter show that uniform silica shells on individual anisotropic NCs are obtained with the reverse microemulsion method if the ammonia concentration is substantially decreased. This approach is expected to work for a variety of anisotropic NCs, provided the native ligands are exchangeable for TEOS. Hence, the results in this chapter represent an important step towards the fabrication of (functionalized) silica-coated NPs with anisotropic shapes.

4. Essential steps towards plastic crystals of silica-coated NRs

4.1 Introduction

Plastic crystals of anisotropic dumbbell-shaped microparticles were recently obtained by van Blaaderen's group.[1-3] In this type of liquid crystal, the particles are at fixed positions with interparticle distances larger than the particles themselves (for instance a screening length of 5 µm was obtained for rods with a length of 3.3 µm).[5] Consequently, the rotational freedom causes orientational disorder of the particles, which can be aligned if an electric field is applied.[1] In Figure 4.1, confocal microscopy micrographs of 2D plastic crystals of PMMA dumbbells dispersed in hexane (left) and decalin (right) are shown.[2] It is clearly visible that these particles display positional order but orientational disorder. Note that, the dumbbells oriented with their length perpendicular to the camera appear as spheres on these images.
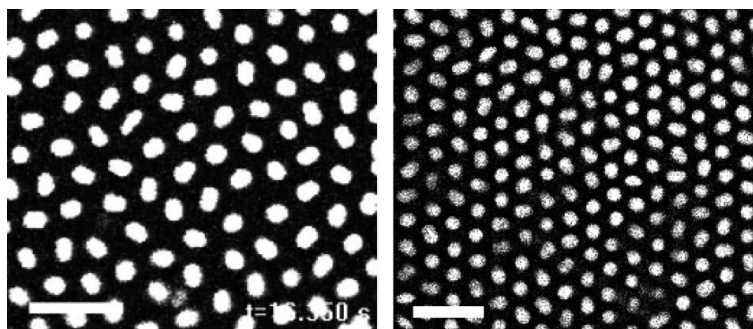

Figure 4.1: Confocal microscopy micrographs of 2D plastic crystals of PMMA dumbbells (diameter ~ 2 µm) in hexane (left) and decalin (right), reproduced from Ref. 2. Scale bars correspond to 10 µm.

This chapter addresses different requirements to achieve the formation of plastic crystals of CdSe/CdS core/shell NRs. Given that these are much smaller than the microparticles previously used for plastic crystals (i.e. a length of ~50 nm instead of ~3 µm), the analysis of plastic crystals with NCs as building blocks remains a challenging target. The main goal of this chapter is hence to design NRs with characteristics essential for the formation of a plastic crystal. Their incorporation in silica provides a crucial first step, since it enlarges their photochemical stability, enables further modification (see chapter three) and furthermore the silica-coated NRs are larger than uncoated NRs. As mentioned in chapter two, long-range repulsion between the dispersed particles is an essential condition for the formation of a plastic crystal. To summarize, the following conditions should therefore be obtained:

- The surface of the NPs is effectively charged (more than 40 mV)
- The solvent is free of (counter-)ions
- The solvent is refractive index-matched with the NPs (n_D = 1.46 for silica)

In this respect, three different methods are compared to transfer the silica-coated NRs from ethanol (ε ~ 24) to solvents with lower dielectric constants (ε < 10) and besides induce sufficient charge on the surface to obtain interparticle distances in the order of a few hundreds of nanometers. The first and most common procedure of hydrophobic modification is by simply grafting the OTMS on the surface, as reported in literature.[54,55,90] In this chapter, grafting is also performed upon addition of TEOS, aiming for a network of silica and OTMS around the silica-coated NRs to induce more charge on each particle. The last method utilizes the reaction cavity inside the w/o microemulsion by adding OTMS towards the end of the silica coating procedure, i.e. if the TEOS is depleted. The ζ-potentials are measured as indication for the surface charge of these NPs in a nonpolar medium.

4.2   Experimental

4.2.1   Chemicals and solvents
Ammonia (11.4 wt% in water), cyclohexane (Sigma-Aldrich, anhydrous, 99%), cyclohexylbromide (CHB, Sigma-Aldrich, 98%), cyclohexylchloride (CHC, Sigma-Aldrich, 99%), ethanol (Alfa Aesar, anhydrous, 96%), n-octadecyltrimethoxysilane (OTMS, fluorochem), tetraethyl orthosilicate (TEOS, Sigma-Aldrich, 99%), toluene (Sigma-Aldrich, anhydrous, 99.8%) were used as supplied. Toluene, CHB and CHC were deionized with molecular sieves (4 Å, Sigma-Aldrich).

4.2.2   Hydrophobic silica-coated NRs
CdSe/CdS core/shell NRs were synthesized as described in paragraphs 3.2.2 & 3.2.3 and coated with silica in a reverse microemulsion with 11.4 wt% ammonia, see paragraph 3.2.7. Experimental details of the syntheses of different samples can be found in Appendix A to C. To make these silica-coated NRs soluble in nonpolar solvents, these were functionalized with OTMS with three different methods. The first was by grafting the silica-coated NCs after these were isolated from the reverse microemulsion (4.2.2.1). The second approach was grafting in presence of TEOS (4.2.2.2) and the final method utilized the reverse microemulsion system to coat the silica-coated NCs with a hydrophobic layer (4.2.2.3). Experimental details are summarized in Appendix D.

4.2.2.1   *Grafting*
The grafting of silica-coated NCs with OTMS was performed by an adapted procedure from literature.[54,55,90] First, 0.12 mL ammonia solution (11.4 wt%) was added to 10 mL of silica-coated NRs in ethanol, prepared as described in paragraph 3.2.6. Then, 1 mL of OTMS in cyclohexane (10%, v/v) was added drop wise to the solution under vigorous stirring (during addition). After 24 hours the particles were separated by centrifugation and redispersed in deionized nonpolar solvent.

4.2.2.2   *Grafting upon addition of TEOS*
Similar to the grafting procedure, 0.12 mL ammonia solution (11.4 wt%) was added to 10 mL silica-coated NRs in ethanol followed by the drop wise addition of 1 mL OTMS in cyclohexane (10%, v/v) with 7 μL TEOS. The resulting particles were separated by centrifugation and redispersed in deionized nonpolar solvent.

4.2.2.3   *Reverse microemulsion method*
The reverse microemulsion was prepared as described in 3.2.7, only one week after ammonia (11.4 wt%) addition, 1 mL of OTMS in cyclohexane (10%, v/v) was added. One day later, the reaction was quenched with ethanol followed by sedimentation. Here, it is assumed that the TEOS is depleted after one week and OTMS after one day: these growth times will be longer at lower ammonia concentrations and vice versa. The resulting particles were washed twice with a toluene/ethanol mixture and finally dispersed in a deionized nonpolar solvent.

4.3   Characterization
To characterize the size and shape of the OTMS-silica-coated NRs, prepared as described in experimental (3.2.2-6 and 4.2.2), TEM images were obtained according to 3.3.1. Furthermore, electrophoresis measurements were performed to determine the ζ-potential of the NPs (4.3.1) and the desired wt% were obtained by dilution of the stock dispersions (4.3.2).

4.3.1   Electrophoresis measurements
The electrophoretic mobilities were measured with diluted dispersions of OTMS-silica-coated NRs in CHC, CHB or toluene using a probe (universal dip cell PCS1115, Malvern) and a Malvern Zetasizer

Nano operating at 25°C. These were converted to the ζ-potential using the Hückel equation (see 2.2.1), averaged over three measurements.

4.3.2 Determination of wt% and conversion to volume fraction

To determine the weight-percentage of a concentrated dispersion of OTMS-silica-coated NRs in a nonpolar solvent, 500 μL was taken and weighed prior to and after evaporation of the solvent. Consequently, these dispersions were diluted to obtain the desired wt% for a plastic crystal with an interparticle center-to-center distance of 300 nm. Therefore, the length and diameter of the silica-coated NRs were calculated with iTEM to which an additional 4.6 nm was added for the OTMS layer.[107] The volume fraction ϕ was calculated with equation 4 (chapter 2) and translated to the wt% of the dispersions by taking into consideration the densities of the NPs and the solvent. Because the calculated volume fractions were lower than 0.003 for the NPs used in this chapter, the contribution of the NPs to the density of the dispersion was neglected and the wt% was calculated according to:

$$wt\% = 100 \frac{\rho_{NP}V_{NP}}{\rho_{TOT}V_{TOT}} = \frac{180\,\phi}{\rho_{solvent}} \qquad (8)$$

With ρ_{NP} the density of the NPs, assumed to be the density of amorphous silica (1.8 gcm^{-3}) and $\rho_{SOLVENT}$ the density of the solvent (in gcm^{-3}).

4.4 Results and discussion

In this paragraph, different modification steps to design NRs suitable for plastic crystals are explored. CdSe/CdS core/shell NRs were synthesized by seeded growth (3.2.2-3), coated with silica according to the standard procedure (3.2.7) and afterwards functionalized with the organosilicon compound OTMS ($(H_3CO)_3SiC_{18}H_{39}$), as described in 4.2.2. The resulting NPs are dispersable in nonpolar solvents.

Silica-coated NRs grafted with OTMS

Figure 4.2 A shows NRs of 23.5 ± 2.7 nm by 4.3 ± 0.6 nm completely incorporated in silica after one week of growth, resulting in ellipsoids with length 50.5 ± 5.6 nm and diameter 34.6 ± 3.3 nm. These were grafted with OTMS (4.2.2.1), quenched after two days of growth and dispersed in the index-matched solvent CHC (n_D = 1.46), followed by selective sedimentation to get rid of clusters. Figure 4.2 B shows a TEM image of the resulting OTMS-silica-coated NRs.
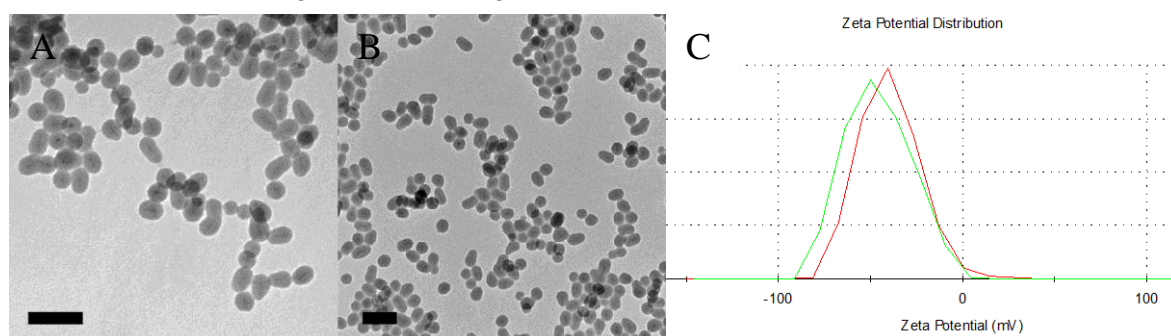
Figure 4.2: A) TEM image of CdSe/CdS core/shell NRs of 23.5 ± 2.7 nm by 4.3 ± 0.6 nm (EMHR01-1) incorporated in silica ellipsoids of 50.5 ± 5.6 nm by 34.6 ± 3.3 nm (EMHS17). B) silica-coated NRs from A after grafting with OTMS (EMHC13). Scale bars correspond to 100 nm. C) two curves of the ζ-potential distribution (a.u.) in CHC of the NPs displayed in B.

From these TEM images can be concluded that the silica shell remained perfectly intact upon this grafting step. The NPs shown in Figure 4.2 B were dispersable in nonpolar solvents (e.g. toluene), indicating that OTMS was successfully grafted on the surface. The OTMS-silica-coated NRs dispersed in CHC displayed a high average ζ-potential (a.u.) of -45.8 ± 17.2 mV, as shown in Figure 4.2. Hence, these modification steps are successful to design NRs that are suitable for plastic crystals.

Silica-coated NRs grafted with a network of OTMS and TEOS

The grafting of silica-coated NRs with OTMS was also performed in presence of TEOS (4.2.2.2). Figure 4.3 shows the silica-coated NRs from Figure 3.2 (one day of growth) grafted with OTMS and TEOS, isolated after one week of growth. A TEM image of the silica-coated NRs prior to grafting is displayed in the left corner for comparison.
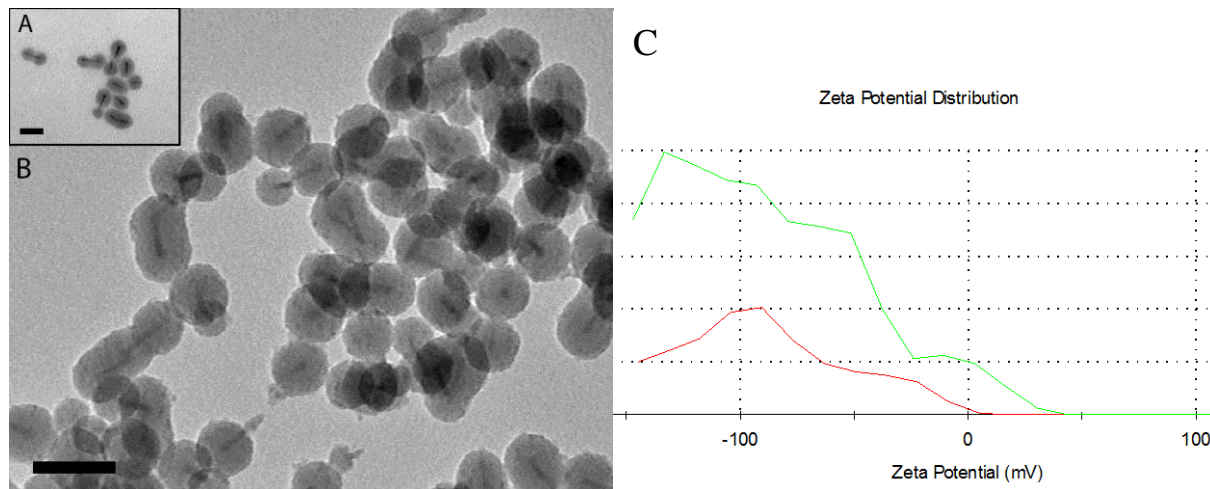

Figure 4.3: TEM images of CdSe/CdS core/shell NRs of 37.1 ± 4.1 nm by 4.3 ± 0.3 nm (130110,2) coated with silica resulting in ellipsoids of 55.6 ± 9.6 by 33.4 ± 2.6 nm prior to (A) and after grafting with OTMS and TEOS (B). The NPs displayed in B are 55.6 ± 5.7 nm by 35.6 ± 2.9 nm. Scale bars correspond to 50 nm. The two curves of the ζ-potential distribution (C) correspond to the OTMS-silica-coated NRs from B.

Figure 4.3 B clearly shows that a rough layer is formed around the silica-coated NRs and accordingly, the diameter of the NPs increased approximately 2 nm in thickness (from 33.4 ± 2.6 nm to 35.6 ± 2.9 nm according to TEM). This confirms that the addition of TEOS during grafting with OTMS leads to enlargement of the silica shell. The NPs grafted with OTMS and TEOS were neither fully dispersable in CHC nor in ethanol, which can be explained considering that there is most likely a network on the surface that consists of both (hydrolyzed) TEOS and OTMS. Both of these compounds attach in a similar manner to the silica shell, i.e. hydrolysis of either an ethoxygroup (TEOS) or methoxygroup (OTMS) followed by condensation, base-catalyzed by the hydroxide ions from the ammonia solution. Therefore, if these attach simultaneously to the silica shell around the NRs, the final surface could be either hydrophilic, hydrophobic or intermediate, depending on whether the outer layer mainly consists of hydroxyl-groups from the silica, hydrocarbon chains from the OTMS or a mixture of these two. In Figure 4.3 C, the ζ-potential distribution (a.u.) of these OTMS-silica-coated NRs in CHC is shown. The averaged ζ-potential of -95.7 ± 46.0 mV is substantially higher than the -45.8 ± 17.2 mV of the NPs from Figure 4.2. In this respect, a possible explanation is that the grafting in presence of TEOS led to an extra layer consisting of silica and OTMS, hence containing relatively large pores (OTMS ~ 2.3 nm). Consequently, the surface area of each NP becomes larger, resulting in a higher surface charge. The broad distribution of the ζ-potential could be due to the fact that the NPs displayed in Figure 4.3 B formed visibly large aggregates instead of stable dispersions in CHC.

Hence, grafting with OTMS and TEOS is a successful method to enlarge silica-coated NCs and without further modification steps the final surface could be highly charged. However, the resulting NPs are relatively hydrophilic compared to the NPs grafted with only OTMS indicated by the poor solubility in CHC. Therefore, grafting with OTMS and TEOS should be further optimized to obtain NPs that are not only highly charged but also fully dispersable in a nonpolar solvent.

NRs coated with silica and further modified with OTMS inside the reverse microemulsion

It needs to be considered that if silica-coated NRs are dispersed in ethanol, these tend to aggregate into large clusters. Hence, it is questionable whether the grafting procedure encapsulates individual or multiple silica-coated NRs with a hydrophobic layer. Therefore, a third method to obtain OTMS-silica-coated NRs was investigated aiming for individual hydrophobic NPs (4.2.2.3). In this respect, OTMS was added to the reverse microemulsion (with more than 11.4 wt% ammonia) before the silica-coated NRs were isolated.

Figure 4.4 A shows NRs of 23.5 ± 2.7 nm by 4.3 ± 0.6 nm coated with silica and OTMS in a reverse microemulsion with 11.4 wt% ammonia, resulting in NPs of 42.8 ± 10 nm by 29.1 ± 2.6 nm. These were successfully dispersable in nonpolar solvents such as toluene and displayed an averaged ζ-potential of -41.2 ± 43.3 mV in toluene (without deionization of the solvent). This is comparable to the surface charge of silica-coated NRs that were grafted with OTMS (Figure 4.2) and dispersed in CHC. Hence, these results show that the reverse microemulsion provides a versatile pathway to directly cover the silica-coated NRs with an additional hydrophobic OTMS shell. This can be understood considering that inside a reverse microemulsion, the micelles behave as reaction cavities in which NCs can be individually coated with silica and in this case also further functionalized with OTMS. Similar to the ethoxy groups of the TEOS monomers (3.4.1), the methoxy groups of OTMS can be hydrolyzed and hence bind covalently to the silica surface by condensation. Consequently, the silica-coated NRs can be directly functionalized with OTMS. Note that, if OTMS is added when there is still (hydrolyzed) TEOS a network of silica and OTMS is expected, while addition of OTMS after depletion of TEOS monomers leads to a completely functionalized surface.
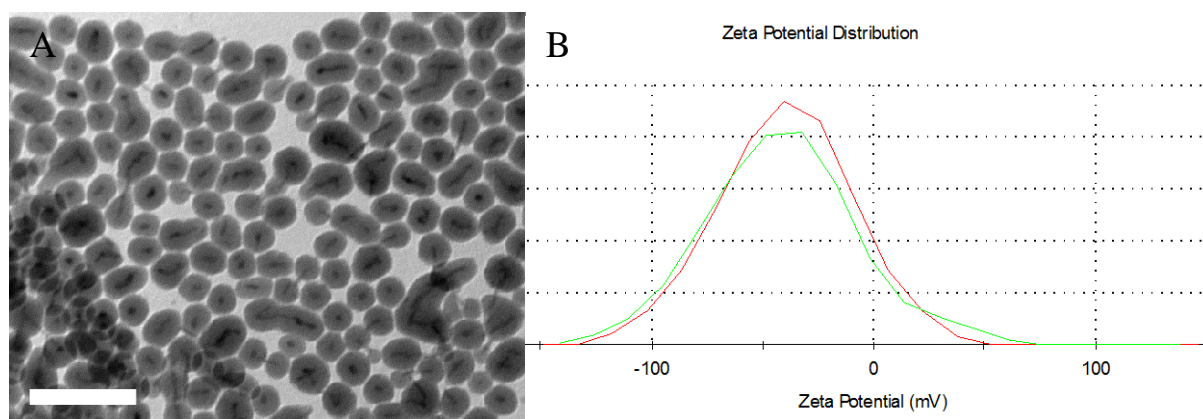
Figure 4.4: OTMS-silica-coated NRs of 42.8 ± 10 nm by 29.1 ± 2.6 nm prepared inside a reverse microemulsion (A) and two curves of the corresponding ζ-potential distribution (a.u.) in toluene (B).

Functionalization of the silica surface with OTMS in the reverse microemulsion was also performed with other NCs such as CdSe NPLs and CdSe/CdS core/shell NPLs (3.4.3 & 4), resulting in NPs dispersable in nonpolar solvents (see Appendix M). Consequently, it is likely that this method is applicable to all types of NCs that can be incorporated in silica with the reverse microemulsion method.

ζ-potentials of OTMS-silica-coated NRs

Altogether, different methods successfully led to the OTMS functionalization of silica-coated NRs that were afterwards dispersed in deionized CHC, CHB or toluene. Table 1 provides an overview of ζ-potentials corresponding to OTMS-silica-coated NRs prepared by different methods. For all these NPs, negative ζ-potentials were measured ranging from -37.4 ± 33.5 mV up to -95.7 ± 46.0 mV. As mentioned in chapter two, a ζ-potential of ~40 mV should be sufficient to induce long-range repulsion. If the solvent is then index-matched with the particles (n_D = 1.46 for silica, CHC and CHB) the

attractive van der Waals forces are minimized. Hence, conditions essential for the formation of a plastic crystal of CdSe/CdS core/shell NRs were obtained via different pathways. The NRs remained photoluminescent after coating with silica and OTMS, see Appendix N, and therefore these results represent a crucial step towards plastic crystals of NC structures.

Sample name	NRs	in SiO$_2$	Method	Solvent	ζ-potential (mV)	SD (mV)	κ (mS/cm)
EMHC05	EMHR01	EMHS08	ME	Toluene	-41.2	34.3	4.08E-04
EMHC08	130110.2	EMHS04	G	CHB	-88.0	21.2	2.07E-04
EMHC09	EMHR01-1	EMHS17	G	CHB	-40.0	26.9	2.49E-04
EMHC10	EMHR01-1	EMHS17	G	CHB	-37.7	20.5	4.75E-04
EMHC11	130110.2	EMHS03	G+T	CHC	-95.7	46.0	3.70E-04
EMHC13	EMHR01-1	EMHS17	G	CHC	-45.8	17.6	1.93E-04
EMHC14	EMHR06-1	EMHS20	G+T	CHC	-68.3	19.5	4.47E-04
EMHC16	EMHR06-1	EMHS20	G	CHC	-94.2	26.1	1.08E-04
EMHC17	EMHR06-1	EMHS26	G	CHC	-81.8	48.1	3.04E-04
EMHC18	EMHR06-1	EMHS30	G	CHC	-62.2	21.2	1.14E-04
EMHC19	EMHR06-1	EMHS31	G	CHC	-37.4	33.5	1.34E-04
EMHC20	EMHR06-1	EMHS32	G	CHC	-54.5	15.4	4.44E-04

Table 1: Summarized ζ-potentials, averaged over three measurements, of OTMS-silica-coated CdSe/CdS core/shell NRs that were used to prepare plastic crystals. The sample names are listed in the first column, followed by the batch of NRs (second column) used to incorporate in silica (third column). The NRs correspond to the TEM images shown in chapter three (3.4.1). Experimental details of the silica coating are in Appendix C. The methods of functionalization with OTMS are also listed: ME is short for microemulsion (4.2.2.3), G for grafting (4.2.2.1) and G+T for grafting upon addition of TEOS (4.2.2.2).

4.5   Conclusion and outlook

In this chapter, silica-coated CdSe/CdS core/shell NRs were successfully functionalized with a hydrophobic ligand (OTMS) via several pathways and the resulting NPs displayed negative ζ-potentials (ranging from -37.4 mV to -95.7 mV) in refractive index-matched nonpolar solvents. Theoretically, the interparticle repulsions corresponding with these surface charges should be ideal to form long-range plastic crystals in diluted dispersions. Hence, the results in this chapter provide essential steps towards the formation of plastic crystals of luminescent CdSe/CdS core/shell NRs that are shielded from the direct environment by silica and thus stable in water- and oxygen-rich environments. However, up to this moment, the analysis of plastic crystals of building blocks in the nanometer size regime remains a challenge. The resolution of the currently available confocal microscope is not high enough to image individual (OTMS-silica-coated) NRs and hence, the possibilities to examine whether plastic crystals are formed are highly limited.

If progress has been made on the confocal microscopy analysis of nanometer-sized objects in solution, the next step is the crystallization of OTMS-silica-coated NCs. Therefore, capillaries should be filled with diluted dispersions of OTMS-silica-coated NRs (in CHB, CHC or toluene) with wt% needed to obtain plastic crystals with interparticle distances in the range of visible light (i.e. 300 nm). A first indication of the successful formation of a crystal in which the NPs display long-range order is visible Bragg reflections originating from the periodicity of the plastic crystal. An analysis technique complementary to confocal microscopy is FIB-SEM imaging, which visualizes cross sections of the contents of the capillary after freezing. In this respect, a dispersion medium should be chosen that does not crystallize upon freezing. Another possibility would be analysis with Small Angle X-ray Scattering (SAXS) to detect periodicity, indicating the interparticle distances in the plastic crystal.

5. Acknowledgments

Bibliography

1. Demirörs, A. F., Johnson, P. M., van Kats, C. M., van Blaaderen, A. & Imhof, A. Directed self-assembly of colloidal dumbbells with an electric field. *Langmuir* **26,** 14466–14471 (2010).

2. Peng, B., Vutukuri, H. R., van Blaaderen, A. & Imhof, A. Synthesis of fluorescent monodisperse non-spherical dumbbell-like model colloids. *J. Mater. Chem.* **22,** 21893–21900 (2012).

3. Peng, B., van Blaaderen, A. & Imhof, A. Direct observation of the formation of liquid protrusions on polymer colloids and their coalescence. *ACS Appl. Mater. Interfaces* **5,** 4277–4284 (2013).

4. Marechal, M. & Dijkstra, M. Stability of orientationally disordered crystal structures of colloidal hard dumbbells. *Phys. Rev. E* **77,** 061405 (1–10) (2008).

5. Liu, B. *et al.* Switching plastic crystals of colloidal rods with electric fields. *Nat. Commun.* **5,** 3092 (2014).

6. Kuijk, A. Fluorescent Colloidal Silica Rods. 40–42 (2012).

7. Peng, B. Control over Colloidal Particle Morphology by Dispersion Polymerization. 151–164 (2013).

8. Vanmaekelbergh, D. Self-assembly of colloidal nanocrystals as route to novel classes of nanostructured materials. *Nano Today* **6,** 419–437 (2011).

9. Wang, T. *et al.* Self-Assembled Colloidal Superparticles from Nanorods. *Science.* **338,** 358–363 (2012).

10. Henzie, J., Grünwald, M., Widmer-Cooper, A., Geissler, P. L. & Yang, P. Self-assembly of uniform polyhedral silver nanocrystals into densest packings and exotic superlattices. *Nat. Mater.* **11,** 131–7 (2012).

11. Srivastava, S. *et al.* Light-controlled self-assembly of semiconductor nanoparticles into twisted ribbons. *Science.* **327,** 1355–1359 (2010).

12. Carbone, L. *et al.* Synthesis and micrometer-scale assembly of colloidal CdSe/CdS nanorods prepared by a seeded growth approach. *Nano Lett.* **7,** 2942–2950 (2007).

13. Pietra, F. *et al.* Semiconductor nanorod self-assembly at the liquid/air interface studied by in situ GISAXS and ex situ TEM. *Nano Lett.* **12,** 5515–5523 (2012).

14. Kagan, C. R. *et al.* Colloidal synthesis of nanocrystals and nanocrystal superlattices. *IBM J. Res. Dev.* **45,** 47–56 (2001).

15. Redl, F. X., Cho, K.-S., Murray, C. B. & O'Brien, S. Three-dimensional binary superlattices of magnetic nanocrystals and semiconductor quantum dots. *Nature* **423,** 968–971 (2003).

16. Chen, Z., Moore, J., Radtke, G., Sirringhaus, H. & O'Brien, S. Binary Nanoparticle Superlattices in the Semiconductor-Semiconductor System: CdTe and CdSe. *J. Am. Chem. Soc.* 1213–1219 (2007).

17. Pileni, M. P. Nanocrystal Self-Assemblies: Fabrication and Collective Properties. *J. Phys. Chem. B* **105,** 3358–3371 (2001).

18. Alivisatos, A. P. Semiconductor Clusters, Nanocrystals, and Quantum Dots. *Science.* **271,** 933–937 (1996).

19. Alivisatos, A. P. Perspectives on the Physical Chemistry of Semiconductor Nanocrystals. *J. Phys. Chem.* **100,** 13226–13239 (1996).

20. Burda, C., Chen, X., Narayanan, R. & El-Sayed, M. A. Chemistry and properties of nanocrystals of different shapes. *Chem. Rev.* **105,** 1025–1102 (2005).

21. Donegá, C. de M. Synthesis and properties of colloidal heteronanocrystals. *Chem. Soc. Rev.* **40,** 1512–1546 (2011).

22.   Talapin, D. V *et al.* Seeded Growth of Highly Luminescent CdSe/CdS Nanoheterostructures with Rod and Tetrapod Morphologies (Supporting Information). *Nano Lett.* **7,** 2951–2959 (2007).

23.   Mahler, B., Nadal, B., Bouet, C., Patriarche, G. & Dubertret, B. Core/shell colloidal semiconductor nanoplatelets. *J. Am. Chem. Soc.* **134,** 18591–18598 (2012).

24.   Talapin, D. V. *et al.* CdSe/CdS/ZnS and CdSe/ZnSe/ZnS Core-Shell-Shell Nanocrystals. *J. Phys. Chem. B* **108,** 18826–18831 (2004).

25.   Selvan, S. T., Tan, T. T. & Ying, J. Y. Robust, Non-Cytotoxic, Silica-Coated CdSe Quantum Dots with Efficient Photoluminescence. *Adv. Mater.* **17,** 1620–1625 (2005).

26.   Selvan, S. T., Patra, P. K., Ang, C. Y. & Ying, J. Y. Synthesis of Silica-Coated Semiconductor and Magnetic Quantum Dots and Their Use in the Imaging of Live Cells. *Angew. Chemie Int. Ed.* **119,** 2500–2504 (2007).

27.   Koole, R. *et al.* On the Incorporation Mechanism of Hydrophobic Quantum Dots in Silica Spheres by a Reverse Microemulsion Method. *Chem. Mater.* **20,** 2503–2512 (2008).

28.   Kittel, C. *Introduction to Solid State Physics Seventh Edition*. 198–228 (1996).

29.   Shriver & Atkins. *Inorganic Chemistry Fourth Edition*. 72–107 (2006).

30.   Nirmal, M. & Brus, L. Luminescence Photophysics in Semiconductor Nanocrystals. *Acc. Chem. Res.* **32,** 407–414 (1999).

31.   Krahne, R. *et al.* Physical properties of elongated inorganic nanoparticles. *Phys. Rep.* **501,** 75–221 (2011).

32.   Peng, X. *et al.* Shape control of CdSe nanocrystals. *Nature* **404,** 59–61 (2000).

33.   Son, J. S. *et al.* Dimension-controlled synthesis of CdS nanocrystals: from 0D quantum dots to 2D nanoplates. *Small* **8,** 2394–2402 (2012).

34.   Shabaev, A. & Efros, A. L. 1D Exciton Spectroscopy of Semiconductor Nanorods. *Nano Lett.* **4,** 1821–1825 (2004).

35.   Ithurria, S. & Dubertret, B. Quasi 2D Colloidal CdSe Platelets with Thicknesses Controlled at the Atomic Level. *J. Am. Chem. Soc.* **130,** 16504–16505 (2008).

36.   Bouet, C. *et al.* Flat Colloidal Semiconductor Nanoplatelets. *Chem. Mater.* **25,** 1262–1271 (2013).

37.   Ithurria, S., Bousquet, G. & Dubertret, B. Continuous Transition from 3D to 1D Confinement Observed during the Formation of CdSe Nanoplatelets. *J. Am. Chem. Soc.* **133,** 3070–3077 (2011).

38.   Li, Z. & Peng, X. Size/shape-controlled synthesis of colloidal CdSe quantum disks: ligand and temperature effects. *J. Am. Chem. Soc.* **133,** 6578–6586 (2011).

39.   Son, J. S. *et al.* Large-scale soft colloidal template synthesis of 1.4 nm thick CdSe nanosheets. *Angew. Chemie* **48,** 6861–6864 (2009).

40.   Wen, X.-D., Hoffmann, R. & Ashcroft, N. W. Two-dimensional CdSe nanosheets and their interaction with stabilizing ligands. *Adv. Mater.* **25,** 261–266 (2013).

41.   Yang, P., Ando, M. & Murase, N. Highly luminescent CdSe/Cd(x)Zn(1-x)S quantum dots coated with thickness-controlled SiO2 shell through silanization. *Langmuir* **27,** 9535–9540 (2011).

42.   Xie, R., Kolb, U., Li, J., Basché, T. & Mews, A. Synthesis and characterization of highly luminescent CdSe-core CdS/ZnCdS/ZnS multishell nanocrystals. *J. Am. Chem. Soc.* **127,** 7480–7488 (2005).

43.   Bertoni, G. *et al.* Direct Determination of Polarity, Faceting, and Core Location in Colloidal Core/Shell Wurtzite Semiconductor Nanocrystals. *ACS Nano* **6,** 6453–6461 (2012).

44. Talapin, D. V *et al.* Highly Emissive Colloidal CdSe/CdS Heterostructures of Mixed Dimensionality. *Nano Lett.* **3,** 1677–1681 (2003).

45. Lunnemann, P. *et al.* Calibrating and controlling the quantum efficiency distribution of inhomogeneously broadened quantum rods by using a mirror ball. *ACS Nano* **7,** 5984–92 (2013).

46. Zhuang, J. *et al.* Cylindrical Superparticles from Semiconductor Nanorods (Supporting Information). *J. Am. Chem. Soc.* **131,** 6084–6085 (2010).

47. Amirav, L. & Alivisatos, A. P. Photocatalytic Hydrogen Production with Tunable Nanorod Heterostructures. *J. Phys. Chem. Lett.* **1,** 1051–1054 (2010).

48. Steiner, D. *et al.* Determination of band offsets in heterostructured colloidal nanorods using scanning tunneling spectroscopy. *Nano Lett.* **8,** 2954–2958 (2008).

49. Hu, J. *et al.* Linearly polarized emission from colloidal semiconductor quantum rods. *Science.* **292,** 2060–2063 (2001).

50. Resch-Genger, U., Grabolle, M., Cavaliere-Jaricot, S., Nitschke, R. & Nann, T. Quantum dots versus organic dyes as fluorescent labels. *Nat. Methods* **5,** 763–775 (2008).

51. Anikeeva, P. O., Halpert, J. E., Bawendi, M. G. & Bulovic, V. Quantum Dot Light-Emitting Devices with Electroluminescence Tunable over the Entire Visible Spectrum. *Nano Lett.* **9,** 2532–2536 (2009).

52. Correa-Duarte, M. A., Giersig, M. & Liz-Marzán, L. M. Stabilization of CdS semiconductor nanoparticles against photodegradation by a silica coating procedure. *Chem. Phys. Lett.* **286,** 497–501 (1998).

53. Ito, Y. *et al.* Crystalline ultrasmooth self-assembled monolayers of alkylsilanes for organic field-effect transistors. *J. Am. Chem. Soc.* **131,** 9396–9404 (2009).

54. Hu, X. & Gao, X. Silica-Polymer Dual Layer-Encapsulated Quantum Dots with Remarkable Stability. *ACS Nano* **4,** 6080–6086 (2010).

55. Hu, X. & Gao, X. Multilayer coating of gold nanorods for combined stability and biocompatibility. *Phys. Chem. Chem. Phys.* **13,** 10028–10035 (2011).

56. Zheng, F. & Hu, B. Preparation of a high pH-resistant AAPTS-silica coating and its application to capillary microextraction (CME) of Cu, Zn, Ni, Hg and Cd from biological samples followed by on-line ICP-MS detection. *Anal. Chim. Acta* **605,** 1–10 (2007).

57. Tan, T. T., Selvan, S. T., Zhao, L., Gao, S. & Ying, J. Y. Size Control, Shape Evolution, and Silica Coating of Near-Infrared-Emitting PbSe Quantum Dots. *Chem. Mater.* **19,** 3112–3117 (2007).

58. Wang, S., Li, C., Yang, P., Ando, M. & Murase, N. Silica encapsulation of highly luminescent hydrophobic quantum dots by two-step microemulsion method. *Colloids Surfaces A Physicochem. Eng. Asp.* **395,** 24–31 (2012).

59. Primera-Pedrozo, O. M., Ates, M. & Arslan, Z. Silica encapsulation of thiol-stabilized lead selenide (PbSe) quantum dots in aqueous solution. *Mater. Lett.* **102-103,** 116–119 (2013).

60. Yi, D. K. *et al.* Silica-coated nanocomposites of magnetic nanoparticles and quantum dots. *J. Am. Chem. Soc.* **127,** 4990–4991 (2005).

61. Hu, X., Zrazhevskiy, P. & Gao, X. Encapsulation of Single Quantum Dots with Mesoporous Silica. *Ann. Biomed. Eng.* **37,** 1960–1966 (2009).

62. Zhang, M., Cushing, B. L. & O'Connor, C. J. Synthesis and characterization of monodisperse ultra-thin silica-coated magnetic nanoparticles. *Nanotechnology* **19,** 085601 (2008).

63. Gerion, D. *et al.* Synthesis and Properties of Biocompatible Water-Soluble Silica-Coated CdSe/ZnS Semiconductor Quantum Dots. *J. Phys. Chem. B* **105,** 8861–8871 (2001).

64. Darbandi, M., Lu, W., Fang, J. & Nann, T. Silica Encapsulation of Hydrophobically Ligated PbSe Nanocrystals. *Langmuir* **22,** 4371–4375 (2006).

65. Stöber, W. & Fink, A. Controlled Growth of Monodisperse Silica Spheres in the Micron Size Range. *J. Colloid Interface Sci.* **26,** 62–69 (1968).

66. Graf, C., Vossen, D. L. J., Imhof, A. & van Blaaderen, A. A General Method To Coat Colloidal Particles with Silica. *Langmuir* **19,** 6693–6700 (2003).

67. López-Quintela, M. . A. A. Synthesis of nanomaterials in microemulsions: formation mechanisms and growth control. *Curr. Opin. Colloid Interface Sci.* **8,** 137–144 (2003).

68. Darbandi, M., Thomann, R. & Nann, T. Single Quantum Dots in Silica Spheres by Microemulsion Synthesis. *Chem. Mater.* **17,** 5720–5725 (2005).

69. Arriagada, F. J. & Osseo-Asare, K. Controlled hydrolysis of tetraethoxysilane in a nonionic water-in-oil microemulsion: a statistical model of silica nucleation. *Colloids Surfaces A Physicochem. Eng. Asp.* **154,** 311–326 (1999).

70. Nann, T. & Mulvaney, P. Single quantum dots in spherical silica particles. *Angew. Chemie Int. Ed.* **43,** 5393–5396 (2004).

71. Jae Kwon, M., Jung, H. & Hoon Park, J. Synthesis and characterization of the CAT's eye-shaped CoO@SiO2 nanoshell aqueous colloids. *J. Phys. Chem. Solids* **73,** 1448–1451 (2012).

72. Pietra, F. *et al.* Synthesis of Highly Luminescent Silica-Coated CdSe/CdS Nanorods. *Chem. Mater.* **25,** 3427–3434 (2013).

73. Kumar, R. *et al.* In vitro and In vivo Optical Imaging Using Water-Dispersible, Noncytotoxic, Luminescent, Silica-Coated Quantum Rods. *Chem. Mater.* **22,** 2261–2267 (2010).

74. Lian, J., Xu, Y., Lin, M. & Chan, Y. Aqueous-phase reactions on hollow silica-encapsulated semiconductor nanoheterostructures. *J. Am. Chem. Soc.* **134,** 8754–8757 (2012).

75. Xu, Y., Lian, J., Mishra, N. & Chan, Y. Multifunctional Semiconductor Nanoheterostructures via Site-Selective Silica Encapsulation. *Small* **9,** 1908–1915 (2013).

76. Sacanna, S. & Pine, D. J. Shape-anisotropic colloids: Building blocks for complex assemblies. *Curr. Opin. Colloid Interface Sci.* **16,** 96–105 (2011).

77. Ye, X. *et al.* Morphologically controlled synthesis of colloidal upconversion nanophosphors and their shape-directed self-assembly. *Proc. Natl. Acad. Sci. U. S. A.* **107,** 22430–22435 (2010).

78. Barua, S. *et al.* Particle shape enhances specificity of antibody-displaying nanoparticles. *Proc. Natl. Acad. Sci. U. S. A.* **110,** 3270–5 (2013).

79. Pal, S., Tak, Y. K. & Song, J. M. Does the antibacterial activity of silver nanoparticles depend on the shape of the nanoparticle? A study of the Gram-negative bacterium Escherichia coli. *Appl. Environ. Microbiol.* **73,** 1712–1720 (2007).

80. Yethiraj, A. & van Blaaderen, A. A colloidal model system with an interaction tunable from hard sphere to soft and dipolar. *Nature* **42,** 513–517 (2003).

81. Royall, C. P., Leunissen, M. E. & van Blaaderen, A. A new colloidal model system to study long-range interactions quantitatively in real space. *J. Phys. Condens. Matter* **15,** 3581–3596 (2003).

82. Velikov, K. P., Zegers, G. E. & van Blaaderen, A. Synthesis and Characterization of Large Colloidal Silver Particles. *Langmuir* **19,** 1384–1389 (2003).

83. O'Brien, R. W. & White, L. R. Electrophoretic mobility of a spherical colloidal particle. *J. Chem. Soc. Faraday Trans. 2* **74,** 1607–1626 (1978).

84. Doane, T. L., Chuang, C.-H., Hill, R. J. & Burda, C. Nanoparticle ζ -potentials. *Acc. Chem. Res.* **45,** 317–26 (2012).

85. Delgado, A. V., González-Caballero, F., Hunter, R. J., Koopal, L. K. & Lyklema, J. Measurement and Interpretation of Electrokinetic Phenomena (IUPAC Technical Report). *Pure Appl. Chem.* **77,** 1753–1805 (2005).

86. Espinosa, C. E., Guo, Q., Singh, V. & Behrens, S. H. Particle charging and charge screening in nonpolar dispersions with nonionic surfactants. *Langmuir* **26,** 16941–16948 (2010).

87. Mock, E. B. & Zukoski, C. F. Determination of Static Microstructure of Dilute and Concentrated Suspensions of Anisotropic Particles by Ultra-Small-Angle X-ray Scattering. *Langmuir* **23,** 8760–8771 (2007).

88. Rossi, L. *et al.* Cubic crystals from cubic colloids. *Soft Matter* **7,** 4139–4142 (2011).

89. Kuijk, A., Byelov, D. V., Petukhov, A. V., van Blaaderen, A. & Imhof, A. Phase behavior of colloidal silica rods. *Faraday Discuss.* **159,** 181–199 (2012).

90. Wang, W., Gu, B., Liang, L. & Hamilton, W. Fabrication of Two- and Three-Dimensional Silica Nanocolloidal Particle Arrays. *J. Phys. Chem. B* **107,** 3400–3404 (2003).

91. Singh, A. & Ryan, K. M. Crystallization of Semiconductor Nanorods into Perfectly Faceted Hexagonal Superstructures. *Part. Part. Syst. Charact.* **30,** 624–629 (2013).

92. Velikov, K. P., van Dillen, T., Polman, A. & van Blaaderen, A. Photonic crystals of shape-anisotropic colloidal particles. *Appl. Phys. Lett.* **81,** 838–840 (2002).

93. Hutter, E. M. *et al.* Method to Incorporate Anisotropic Semiconductor Nanocrystals of All Shapes in an Ultrathin and Uniform Silica Shell. *Chem. Mater.* **26,** 1905–1911 (2014).

94. Pope, E. J. A. & Mackenzie, J. D. Sol-gel processing of silica II. The role of the catalyst. *J. Non. Cryst. Solids* **87,** 185–198 (1986).

95. Arriagada, F. J. & Osseo-Asare, K. Synthesis of Nanosize Silica in a Nonionic Water-in-Oil Microemulsion: Effects of the Water/Surfactant Molar Ratio and Ammonia Concentration. *J. Colloid Interface Sci.* **211,** 210–220 (1999).

96. Brinker, C. J. Hydrolysis and Condensation of Silicates: Effects on Structure. *J. Non. Cryst. Solids* **100,** 31–50 (1988).

97. Anderson, N. C., Hendricks, M. P., Choi, J. J. & Owen, J. S. Ligand Exchange and the Stoichiometry of Metal Chalcogenide Nanocrystals: Spectroscopic Observation of Facile Metal-Carboxylate Displacement and Binding. *J. Am. Chem. Soc.* (2013). doi:10.1021/ja4086758

98. Wuister, S. F., Swart, I., Driel, F. Van, Hickey, S. G. & Donega, C. D. M. Highly Luminescent Water-Soluble CdTe Quantum Dots. *Nano Lett.* **3,** 503–507 (2003).

99. Mokari, T., Sztrum, C. G., Salant, A., Rabani, E. & Banin, U. Formation of asymmetric one-sided metal-tipped semiconductor nanocrystal dots and rods. *Nat. Mater.* **4,** 855–863 (2005).

100. Mokari, T., Rothenberg, E., Popov, I., Costi, R. & Banin, U. Selective growth of metal tips onto semiconductor quantum rods and tetrapods. *Science.* **304,** 1787–1790 (2004).

101. Ithurria, S. *et al.* Colloidal nanoplatelets with two-dimensional electronic structure. *Nat. Mater.* **10,** 936–941 (2011).

102. Bouet, C. *et al.* Two-Dimensional Growth of CdSe Nanocrystals, from Nanoplatelets to Nanosheets. *Chem. Mater.* **25,** 639–645 (2013).

103. Tessier, M. D., Javaux, C., Maksimovic, I., Loriette, V. & Dubertret, B. Spectroscopy of single CdSe nanoplatelets. *ACS Nano* **6,** 6751–6758 (2012).

104. Son, J. S. *et al.* Colloidal Synthesis of Ultrathin Two-Dimensional Semiconductor Nanocrystals. *Adv. Mater.* **23,** 3214–3219 (2011).

105. Pastoriza-Santos, I., Pérez-Juste, J. & Liz-Marzán, L. M. Silica-Coating and Hydrophobation of CTAB-Stabilized Gold Nanorods. *Chem. Mater.* **18,** 2465–2467 (2006).

106. Peng, Z. A. & Peng, X. Mechanisms of the Shape Evolution of CdSe Nanocrystals. *J. Am. Chem. Soc.* **123,** 1389–1395 (2001).

107. Singh, S., Sasaki, D. Y., Cesarano, J. & Hurd, A. J. Nanometer pores in ultrathin silica films prepared by self-assembly of organic spacers in an alkylsiloxane monolayer. *Thin Solid Films* **339,** 209–215 (1999).

Appendix A

Sample name	Date	TOPO	ODPA	CdO	Se	TOP	TOP2	T (°C)
EMH01	18-2-2013	3.17	0.33	0.07	0.06	0.36	1.12	360
EMH03	28-2-2013	3.01	0.30	0.09	0.07	0.37	1.48	365
EMH04	11-3-2013	3.04	0.34	0.06	0.08	0.54	1.48	355
EMH05	28-3-2013	3.422	0.346	0.057	0.065	0.426	1.48	360
EMH06	27-6-2013	3.08	0.306	0.06	0.06	0.37	1.25	350

This table shows details of the syntheses of CdSe QDs that were prepared as described in 3.2.2. All numbers represent the amounts in grams. The temperature listed in the last column was the measured temperature at the moment of injection.

Appendix B

Sample name	Date	Seeds	TOPO	ODPA	CdO	S	TOP	TOP	Time
EMHR01	26-2-2013	FP160912	3.30	0.30	0.08	0.12	1.50	1.50	8
EMHR03	7-3-2013	FP160912	3.10	0.28	0.10	0.11	1.51	1.50	12
EMHR04	14-3-2013	EMH04	3.37	0.32	0.10	0.12	1.50	1.50	8
EMHR05	20-3-2013	EMH04	3.26	0.33	0.09	0.13	1.51	1.26	8
EMHR06	3-4-2013		3.01	0.324	0.08	0.114	1.45	1.42	8
EMHR07	9-4-2013		3.12	0.35	0.098	0.117	1.52	1.24	7
EMHR08	18-4-2013		3.01	0.331	0.08	0.117	1.57	1.20	12
EMHR09	19-4-2013		3.174	0.312	0.084	0.14	1.51	1.58	12
EMHR10	30-5-2013		4.666	0.445	0.095	0.184	2.224	1.5	11

This table shows details of the syntheses of CdSe/Cds core/shell NRs that were prepared as described in 3.2.3. All numbers represent the amounts in grams. The measured injection temperature in between 350 and 355 °C for all samples. The growth times in minutes are listed in the last column. The seeds starting with EMH correspond to the samples from Appendix A, the names starting with 'FP' were synthesized by Francesca Pietra.

Appendix C

Sample name	Date	Sample NPs	Vol. (µL)	Method	TEOS (µL)	NH$_3$ (µL)	[NH3] (wt%)
EMHS01	19-feb-13	FP130110.2	100	ME	80	150	11.4
EMHS02	19-feb-13	FP130110.2	100	ME	80	150	11.4
EMHS03	19-feb-13	FP130110.2	100	ME	80	150	11.4
EMHS04	19-feb-13	FP130110.2	100	ME	80	150	11.4
EMHS05	6-mrt-13	EMHR01	100	ME	80	150	11.4
EMHS06	6-mrt-13	EMHR01	100	ME	80	150	11.4
EMHS07	6-mrt-13	EMHR01	100	ME	20		11.4
EMHS08	12-mrt-13	EMHR01	100	ME	80	150	11.4
EMHS09	12-mrt-13	EMHR01	100	ME	80	150	11.4
EMHS10	12-mrt-13	EMHR01	100	ME	80	150	11.4
EMHS11	12-mrt-13	EMHR01	100	ME	80	150	11.4
EMHS12	18-mrt-13	EMHR01-1	180	ME	80	150	11.4
EMHS13	18-mrt-13	EMHR01-1	180	ME	80	150	11.4
EMHS14	18-mrt-13	EMHR01-1	180	ME	80	150	11.4
EMHS15	18-mrt-13	EMHR01-1	180	ME	80	150	11.4
EMHS16	22-mrt-13	EMHR01-1	50	ME	80	150	11.4
EMHS17	22-mrt-13	EMHR01-1	50	ME	80	150	11.4
EMHS18	27-mrt-13	EMHR01-1	50	S	80	600	11.4
EMHS19	27-mrt-13	EMHR01-3	50	S	80	600	11.4
EMHS20	10-apr-13	EMHR06	100	ME	80	150	11.4
EMHS21	10-apr-13	EMHR01-1	50	ME	80	150	11.4
EMHS22	10-apr-13	EMHS03		ME	80?	150	11.4
EMHS23	10-apr-13	EMHS03		S	7	75	11.4
EMHS24	23-apr-13	EMHC07	1000	ME	7	150	11.4
EMHS25	23-apr-13	EMHS03	2000	ME	7	150	11.4
EMHS26	23-apr-13	EMHR06	90	ME	80	150	11.4
EMHS27	23-apr-13	EMHR07	90	ME	80	150	11.4
EMHS28	26-apr-13	EMHR08	80	ME	80	150	11.4
EMHS29	26-apr-13	EMHR09	80	ME	80	150	11.4
EMHS30	3-may-13	EMHR06	100	ME	80	150	11.4
EMHS31	3-may-13	EMHR06	100	ME	80	150	11.4
EMHS32	3-may-13	EMHR06	100	ME	80	150	11.4
EMHS33	3-may-13	EMHR06	100	ME	80	150	11.4
EMHS34	27-may-13	EMHR06-1	200	ME	80	150	?
EMHS35	27-may-13	EMHR06-1	200	ME	80	150	?
EMHS36	27-may-13	EMHR08-1	150	ME	80	150	?
EMHS37	31-may-13	EMHS16	2000	S	7	75	11.4
EMHS38	31-may-13	EMHS16	2000	S	7	75	11.4
EMHS39	5-jun-13	EMHR08-1	150	ME	80	150	11.4
EMHS40	5-jun-13	EMHR08-1	150	ME	80	150	8.7
EMHS41	5-jun-13	EMHR08-1	150	ME	80	150	5.7

EMHS42	5-jun-13	EMHR08-1	150	ME	80	150	2.8
EMHS43	13-jun-13	EMHR08-1	150	ME	80	150	11.4
EMHS44	13-jun-13	EMHR08-1	150	ME	80	150	2.8
EMHS45	13-jun-13	EMHR08-1	150	ME	80	150	1.1
EMHS46	13-jun-13	EMHR08-1	150	ME	80	150	0.6
EMHS47	13-jun-13	EMHR08-1	150	ME	80	50	11.4
EMHS48	13-jun-13	EMHR08-1	150	ME	80	200	11.4
EMHS49	20-jun-13	EMHR08-1	150	ME	80	x	
EMHS50	20-jun-13	EMHR08-1	150	ME	80	x	
EMHS51	4-jul-13	D230713	100	ME	80	150	0.6
EMHS52	4-jul-13	D CdSeCdS	500	ME	80	150	0.6
EMHS53	1-aug-13	EMHR08-1	150	ME	80	150	29.9
EMHS54	1-aug-13	EMHR08-1	150	ME	80	150	1.5
EMHS55	1-aug-13	EMHR06-1	400	ME	80	150	29.9
EMHS56	1-aug-13	EMHR06-1	400	ME	80	150	1.5
EMHS57	1-aug-13	D CdSe 1sp4	200	ME	80	150	1.5
EMHS58	1-aug-13	RM247	20	ME	80	150	1.5
EMHS59	6-aug-13	RM247 (S)	20	ME	80	150	0.7
EMHS60	6-aug-13	RM247 (M)	30	ME	80	150	0.7
EMHS61	6-aug-13	RM247 (L)	20	ME	80	150	0.7
EMHS62	6-aug-13	D CdSe 1sp4	250	ME	80	150	0.7
EMHS63	10-aug-13	EMHR06-1	400	ME	80	150	1.5
EMHS64	10-aug-13	EMHR06-1	400	ME	80	150	1.5
EMHS65	11-aug-13	D290413	130	ME	80	150	29.9
EMHS66	11-aug-13	D290413	130	ME	80	150	1.5
EMHS67	11-aug-13	D290413	130	ME	80	75	1.5
EMHS68	11-aug-13	D CdSe 1sp4	250	ME	80	150	0.7
EMHS69	11-aug-13	D CdSe 1sp4	250	ME	80	75	0.7
EMHS70	21-aug-13	D290413	200	ME	80	75	1.5
EMHS71	27-aug-13	D290413	200	ME	80	75	1.5
EMHS72	9-sep-13	D220413	200	ME	80	150	29.9
EMHS73	9-sep-13	D220413	200	ME	80	150	1.5
EMHS74	9-sep-13	D220413	200	ME	80	75	1.5
EMHS75	9-sep-13	D290413	400	ME	80	75	1.5
EMHS76	10-sep-13	EMHR06-1	400	ME	80	75	3
EMHS77	16-sep-13	D220413	200	ME	40	150	29.9
EMHS78	16-sep-13	D220413	200	ME	80	150	29.9
EMHS79	16-sep-13	D290413	400	ME	80	150	1.5
EMHS80	16-sep-13	D070513	600	ME	80	150	1.5
EMHS81	19-sep-13	EMHR08-1	150	ME	80	150	29.9
EMHS82	19-sep-13	A39	400	ME	80	150	1.5
EMHS83	19-sep-13	A39	400	ME	80	150	1.5
EMHS84	26-sep-13	D020513	1000	ME	80	150	29.9
EMHS85	26-sep-13	D020513	1000	ME	80	150	1.5
EMHS86	26-sep-13	A62	2000	ME	80	150	29.9

EMHS87	26-sep-13	A62	2000	ME	80	150	1.5
EMHS88	1-oct-13	QA038	200	ME	80	150	29.9
EMHS89	1-oct-13	QA038	200	ME	80	150	1.5
EMHS90	1-oct-13	D220413	400	ME	80	150	3
EMHS91	1-oct-13	D290413	400	ME	80	150	29.9
EMHS92	11-oct-13	EMHR08-1	150	ME	80	150	1.5
EMHS93	11-oct-13	EMHR08-1	150	ME	80	150	3.7
EMHS94	11-oct-13	EMHR08-1	150	ME	80	150	7.4
EMHS95	11-oct-13	EMHR08-1	150	ME	80	150	15
EMHS96	24-oct-13	EMHR08-1	150	ME	80	75	1.5
EMHS97	12-nov-13	FP131023	100	ME	80	150	1.5
EMHS98	12-nov-13	FP131023	100	ME	80	150	0.7
EMHS99	12-nov-13	Au4	100	ME	80	150	1.5
EMHS100	12-nov-13	Au5	100	ME	80	150	1.5
EMHS101	20-nov-13	Au5	120	ME	80		
EMHS102	20-nov-13	Au4	200	ME	80		
EMHS103	19-dec-13	D220413	400	ME	80	150	3
EMHS104	19-dec-13	AB021-1	400	ME	80	150	3

This table summarizes the silica coating procedure of different types of NCs, as described in 3.2.7. The third column lists the type of NCs: sample names starting with EMH correspond to the NRs from Appendix B, whereas sample names starting with AB, D, FP, RM and QA were synthesized by Annelies van der Bok, Dariusz Mitoraj, Francesca Pietra, Relinde Moes and Quinten Akkerman, respectively.

Appendix D

Sample name	Date	Method	Type of NPs	Silica coating	V	NH₃	OTMS	Growth
EMHC01	8-mar-13	ME	EMHR01	EMHS05	6	0.1	0.5	3 days
EMHC02	8-mar-13	G	EMHR01	EMHS05	2	0.025	0.16	3 days
EMHC03	8-mar-13	G	EMHR01	EMHS05	2	0.025	0.1	3 days
EMHC04	8-mar-13	G	EMHR01	EMHS05	2	0.025	0.05	3 days
EMHC05	13-mar-13	ME	EMHR01	EMHS08	x	0.15	1	1 day
EMHC06	13-mar-13	ME	EMHR01	EMHS09	x	0.15	2	1 day
EMHC07	25-mar-13	G	EMHR01	EMHS11	10	0.12	1	1 day
EMHC08	27-mar-13	G	130110.2	EMHS04	10	0.12	1	1 day
EMHC09	2-apr-13	G	EMHR01-1	EMHS17	2.5	0.03	0.25	1 day
EMHC10	2-apr-13	G	EMHR01-1	EMHS17	2.5	0.03	0.5	1 day
EMHC11	10-apr-13	G + T	130110.2	EMHS03	2	0.075	0.6	7 days
EMHC12	15-apr-13	G	EMHR01-1	EMHS17	2.5	0.03	0.75	2 days
EMHC13	23-apr-13	G	EMHR01-1	EMHS17	2	0.03	0.6	2 days
EMHC14	23-apr-13	G + T	EMHR06	EMHS20	2.5	0.03	0.75	8 days
EMHC15	26-apr-13	ME	EMHR06	EMHS26	6	0.075	1.8	5 days
EMHC16	29-apr-13	G	EMHR06	EMHS20	2.5	0.03	0.75	2 days
EMHC17	13-may-13	G	EMHR06	EMHS26	5	0.06	0.5	1 day
EMHC18	15-may-13	G	EMHR06	EMHS30	10	0.12	1	
EMHC19	15-may-13	G	EMHR06	EMHS31	10	0.12	2	
EMHC20	15-may-13	G	EMHR06	EMHS32	10	0.12	3	
EMHC21	3-jun-13	ME	EMHR06	EMHS34	x	0.15	1	3 days
EMHC23	1-aug-13	G	EMHR06	EMHS33	10	0.12	1	1 day
EMHC24	6-aug-13	ME	EMHR06-1	EMHS55	6	0.075	0.5	2 days
EMHC25	11-aug-13	ME	EMHR06-1	EMHS63	x	0.15	1	
EMHC26	10-sep-13	ME	EMHR06-1	EMHS76	x	0.15	1	3 days
EMHC27	16-sep-13	ME	D220413	EMHS77	x	0.15	1	3 days

This table shows details of the OTMS coating of silica-coated NCs. The sample names listed in the fourth and fifth column of this table correspond to the samples from Appendix B and C, respectively. All numbers represent the volume in mL, in which:

- V the volume of the starting solution in ethanol, assuming 10 mL was added to the total synthesis of silica-coated NCs
- 'x' is the total volume of the microemulsion
- NH₃ an ammonia solution of 11.4 wt% (except for EMHC23 to 27, i.e. 29.9 wt%)
- OTMS is a 10% (v/v) solution in cyclohexane

Appendix E
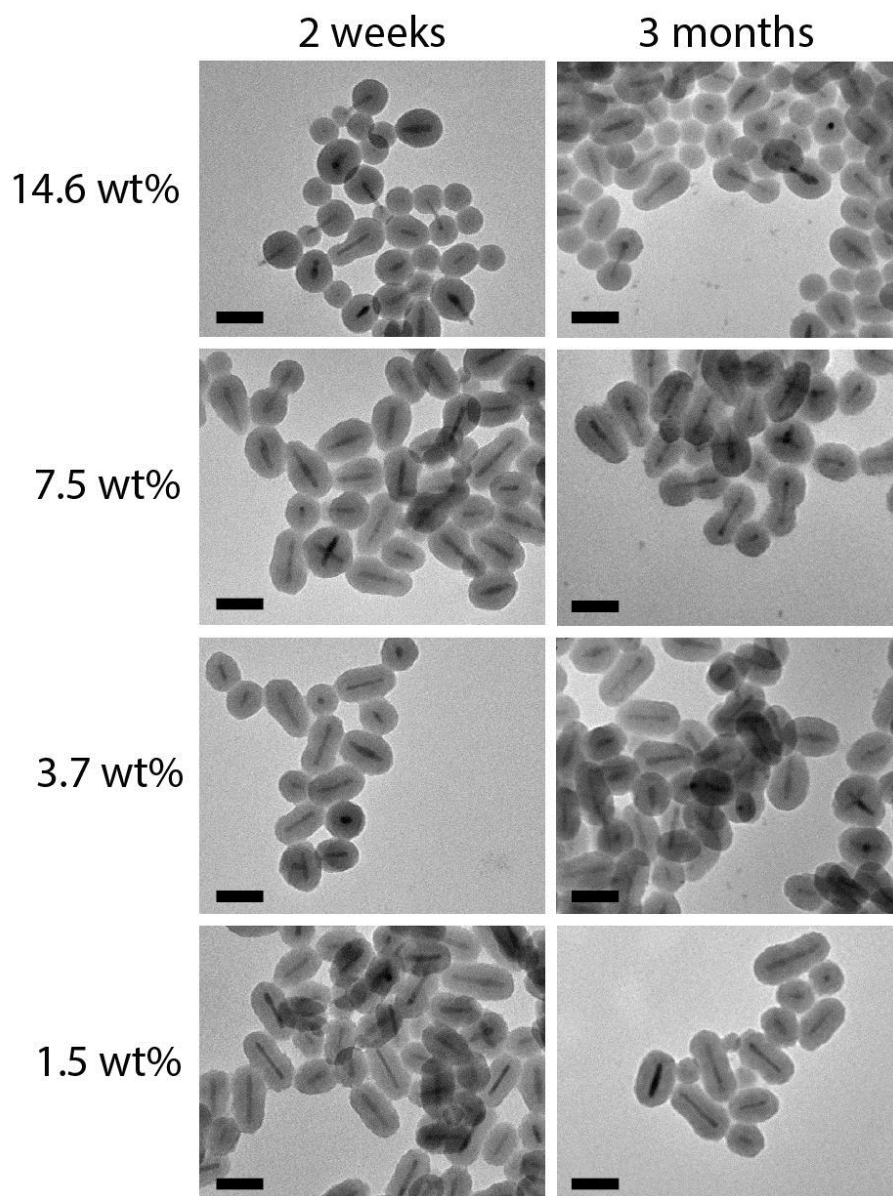
TEM overview of CdSe/CdS core/shell NRs of 48.5 ± 6.3 nm by 6.2 ± 0.9 nm coated with silica in reverse microemulsions with different ammonia concentrations in the aqueous phase, quenched after two weeks (left column) and three months of growth (right column). Scale bars correspond to 50 nm.
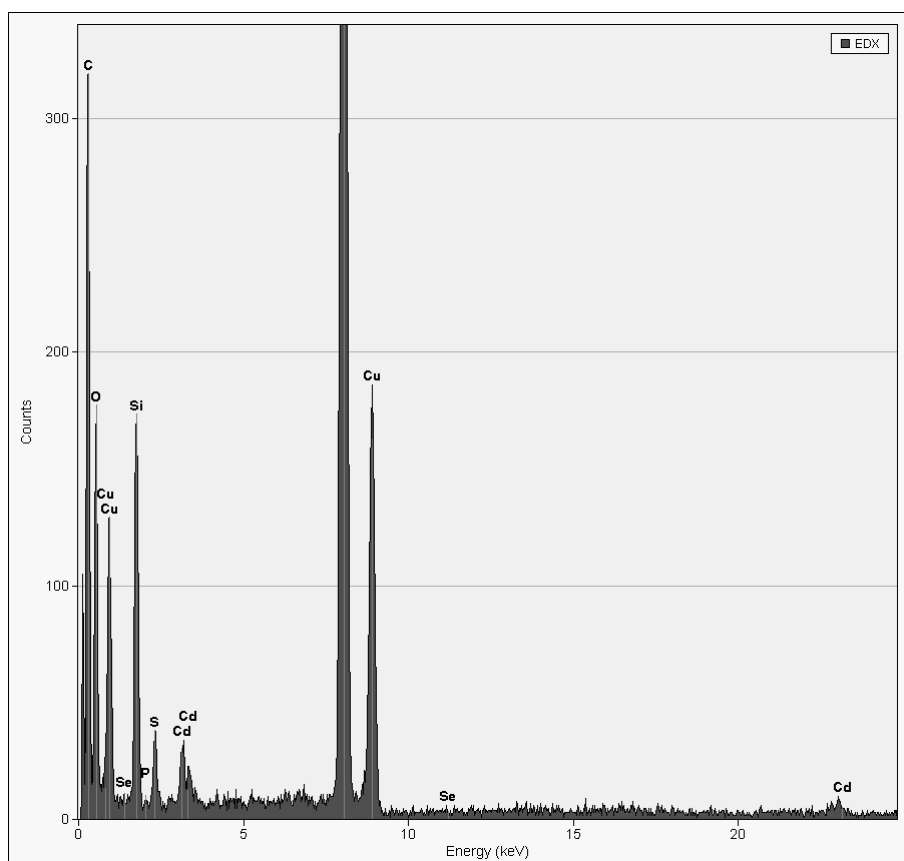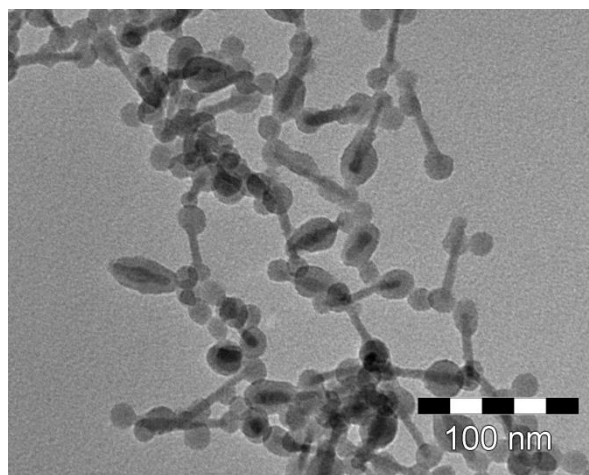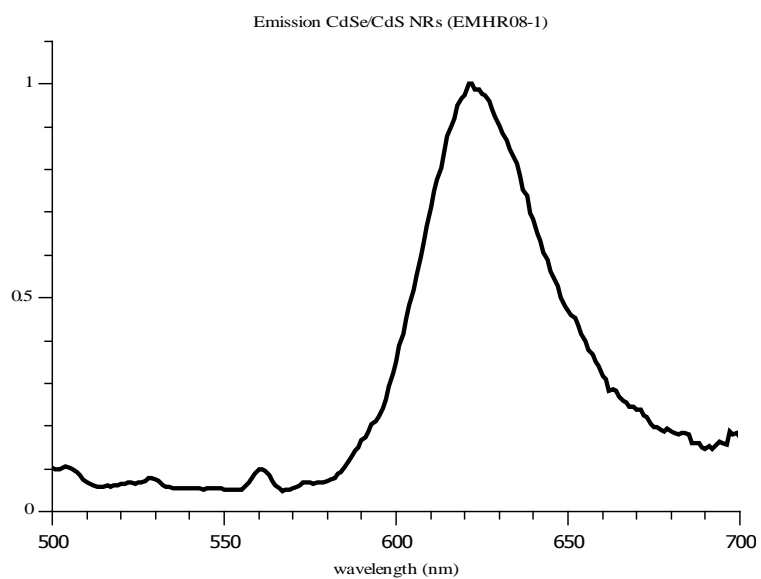
Appendix F
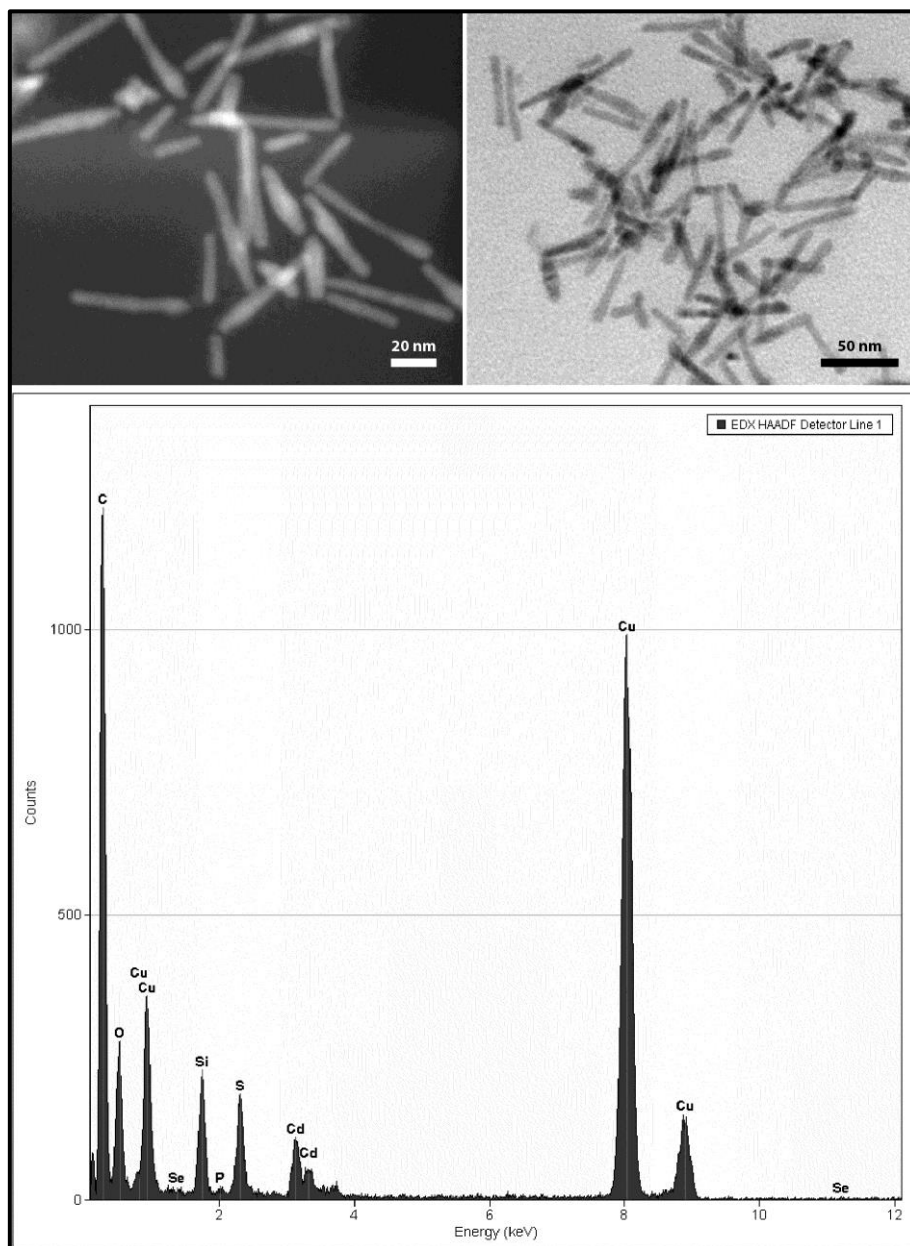
HAADF-STEM (left) and TEM (right) image and corresponding EDX analysis on a group of NRs isolated after 2 hours from a microemulsion with 1.1 wt% ammonia. The presence of phosphor (P) and silicon (Si) confirms that at this stage, both the original capping ligand (ODPA) and TEOS monomers or small silica nuclei are on the surface of the NRs. The elements carbon and copper originate from the TEM-grid.

Appendix G
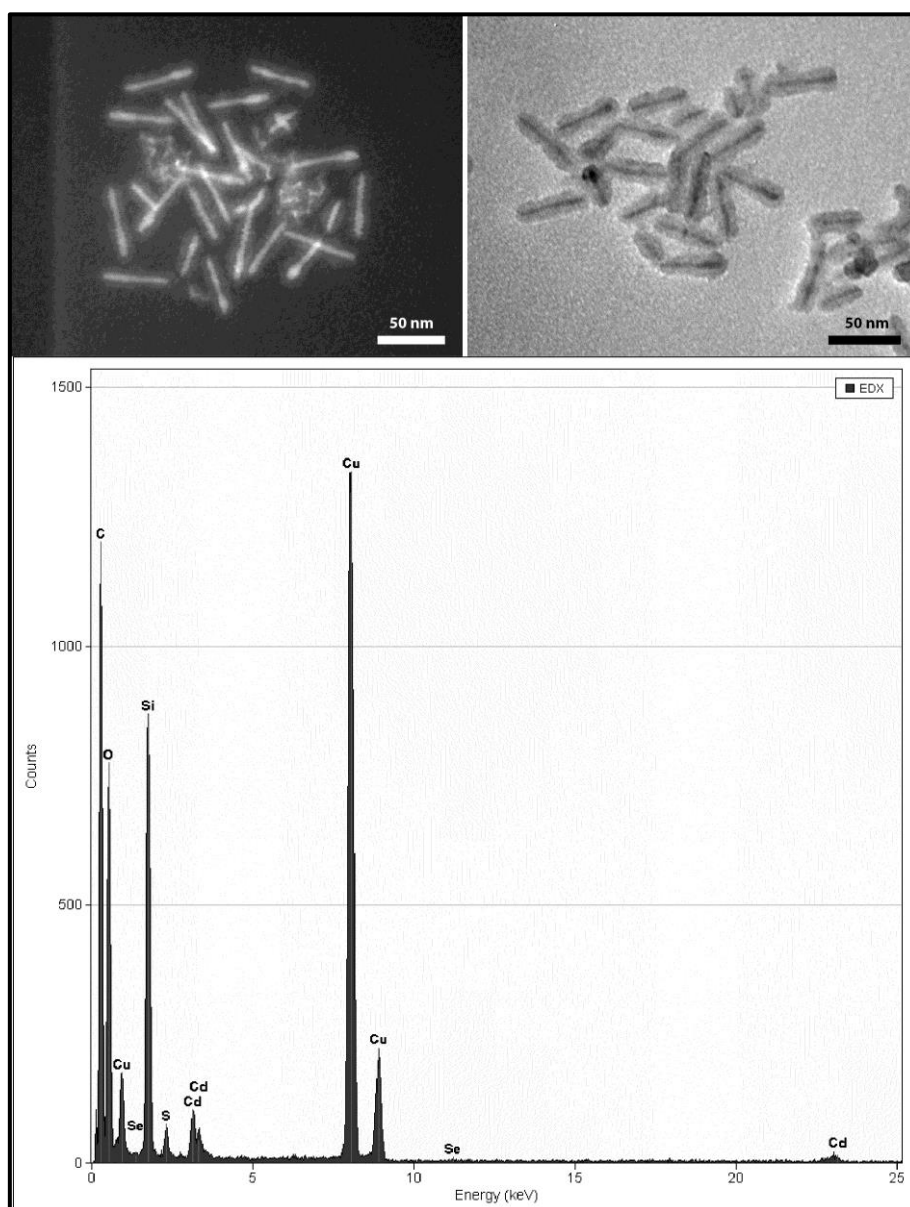
HAADF-STEM (left) and TEM (right) image and corresponding EDX analysis on a group of NRs isolated after 24 hours from a microemulsion with 1.5 wt% ammonia. The absence of phosphor confirms that, at this stage, the original capping ligand is removed from the surface of the NRs.

Appendix H

TEM (right) image and corresponding EDX analysis on a group of NRs isolated after 1 day from a microemulsion with 29.9 wt% ammonia. The presence of phosphor (P) and silicon (Si) confirms that at this stage, both the original capping ligand (ODPA) and TEOS monomers or small silica nuclei are on the surface of the NRs. The elements carbon and copper originate from the TEM-grid.

Appendix I

Emission spectrum of CdSe/CdS core/shell NRs in toluene with emission at 622 nm, sample name corresponds to the image from Figure 3.1

Appendix J
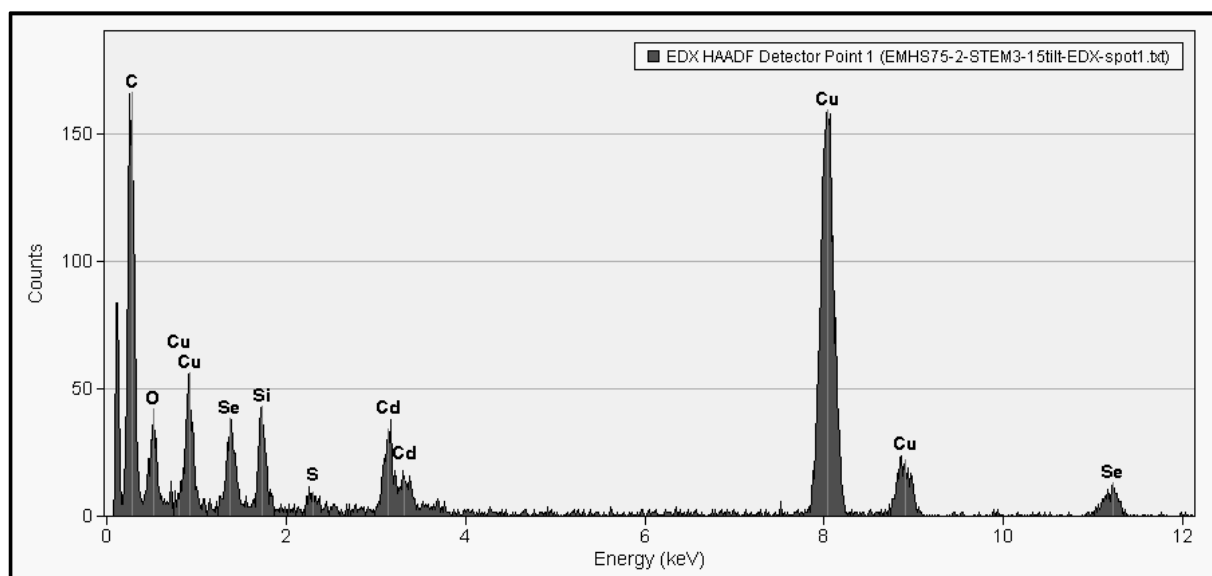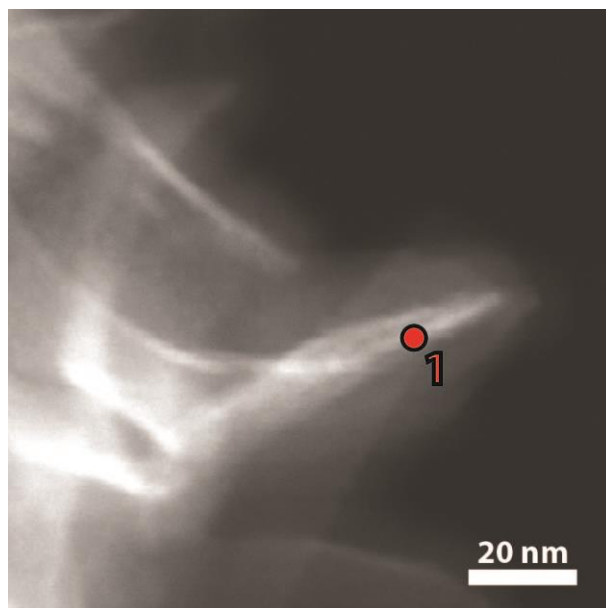
HAADF-STEM image and corresponding EDX analysis on a CdSe/CdS NPL isolated after 24 hours from a microemulsion with 1.5 wt% ammonia, at the spot indicated with '1'. The presence of sulphur (S) suggests that the CdS monolayer stayed intact during the silica coating procedure.

Appendix K
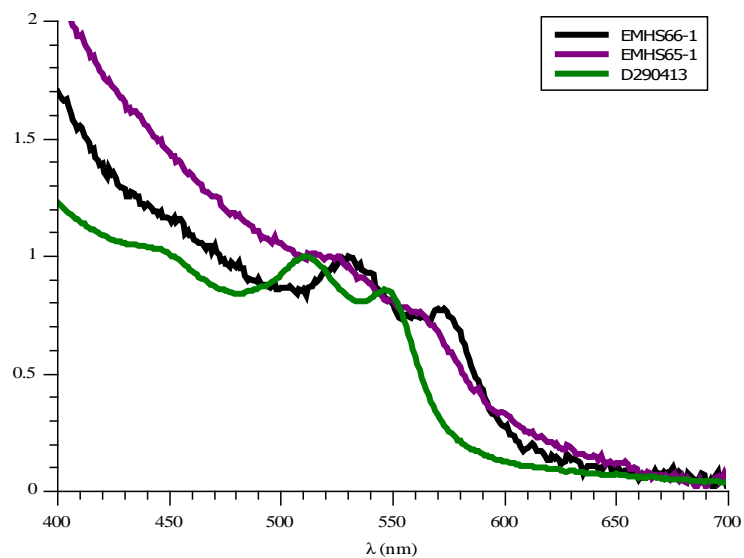
Absorption spectra of CdSe/CdS core/shell NPLs prepared as described in 3.2.5 & 6 prior to (green line, D290413) and after silica coating with 29.9 wt% ammonia (purple line, EMHS65-1) and 1.5 wt% ammonia (black line, EMHS66-1), both quenched after three hours of growth. Comparable to the CdSe NPLs (Figure 3.15), the absorption spectrum is shifted towards the red after coating with silica.

Appendix L
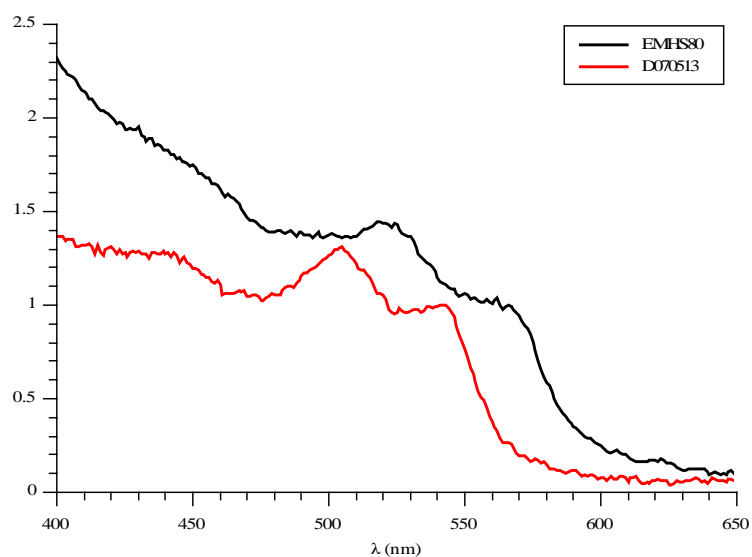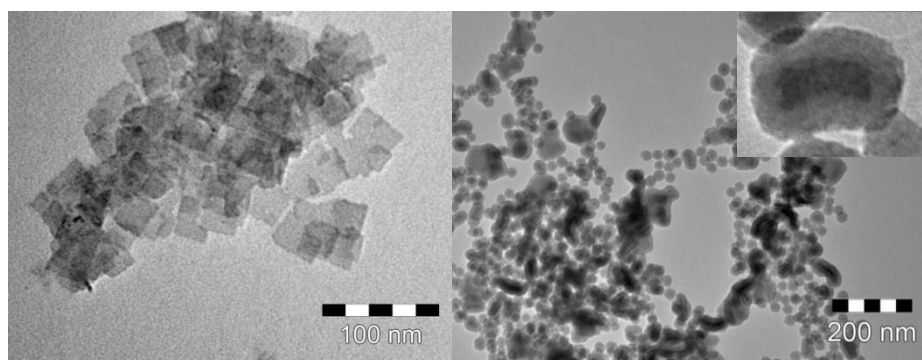
TEM images and corresponding absorption spectra of square CdSe NPLs synthesized according to Li *et al.*[38] with a CdS shell grown as described in 3.2.6 prior to (left image, red line, D070513) and after silica coating with 1.5 wt% ammonia (right image, black line, EMHS66-1), quenched after three hours of growth. This confirms that the low ammonia approach is also applicable to obtain uniform silica shells on 2D NCs that are prepared via a different pathway. The absorption spectra show that also for these NCs, a red-shift after silica coating is observed. Whether this is due to the different environment should be confirmed in follow-up studies.

Appendix M
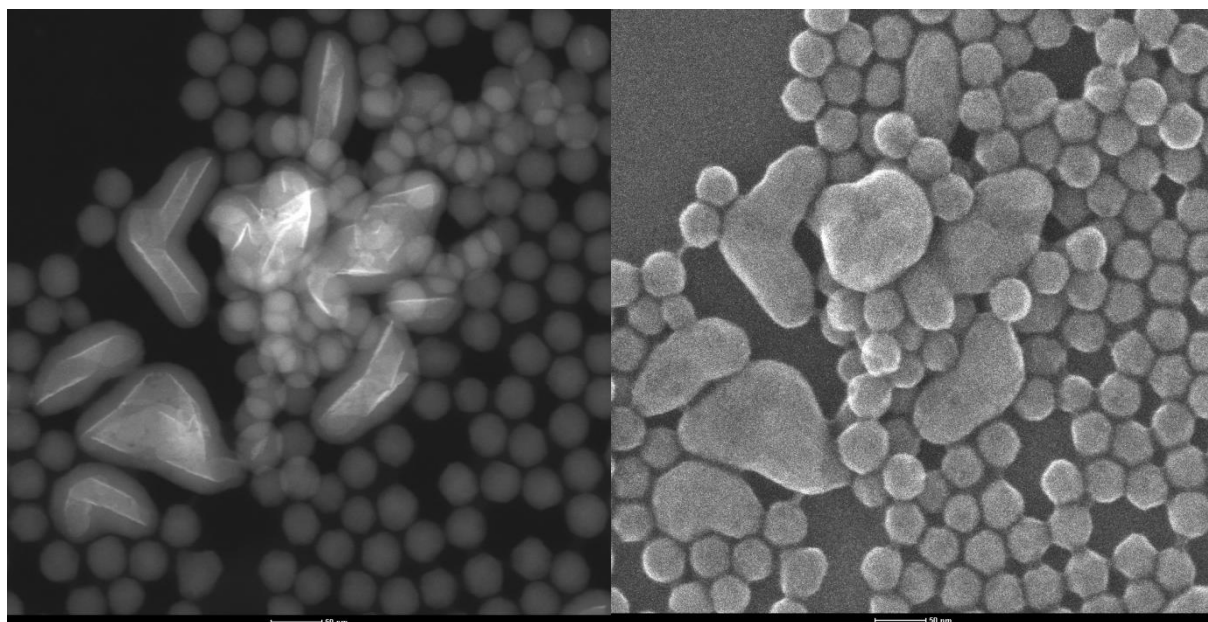
OTMS-silica-coated CdSe NPLs in toluene, prepared according to the microemulsion method from 4.2.2.1. The left image shows a HAADF-STEM image with corresponding SEM image on the right. The high ammonia concentration (29.9 wt%) resulted in helix-shaped NPLs in silica. On the SEM image, it is clearly visible that the incorporation of multiple (attached) NPLs leads to a completely covering anisotropic silica shell. Scale bars correspond to 50 nm.

Appendix N

Emission OTMS-silica-coated NRs (EMHC18) in CHC
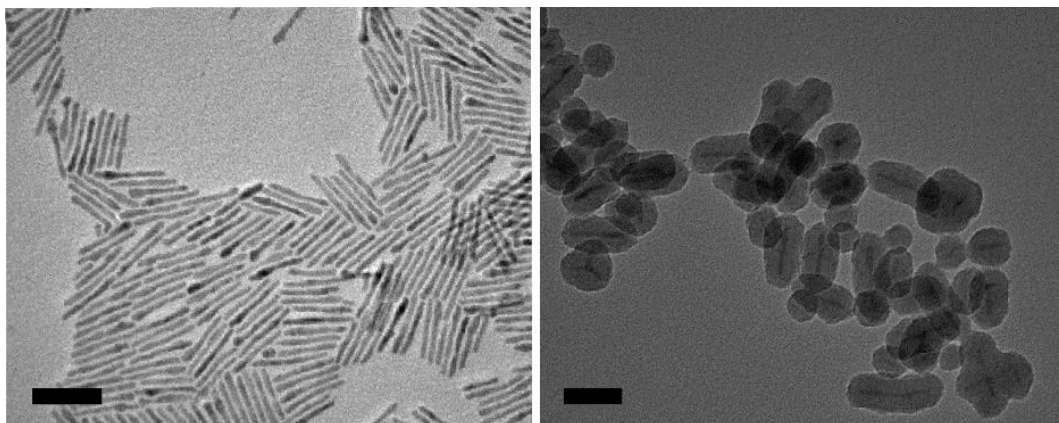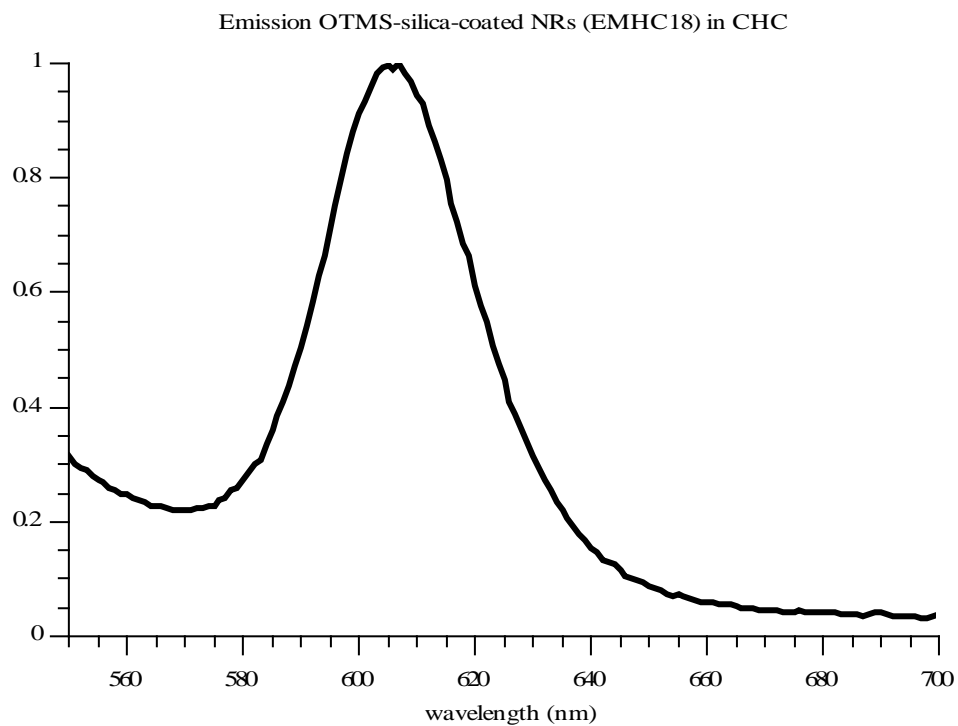
Emission spectrum (a.u.) of OTMS-silica-coated CdSe/CdS core/shell NRs in CHC with emission maximum at 607 nm, the TEM images correspond to the NRs prior to (left, EMHR06-1) and after (right, EMHC18) coating with silica and OTMS. Scale bars represent 50 nm.

Appendix O
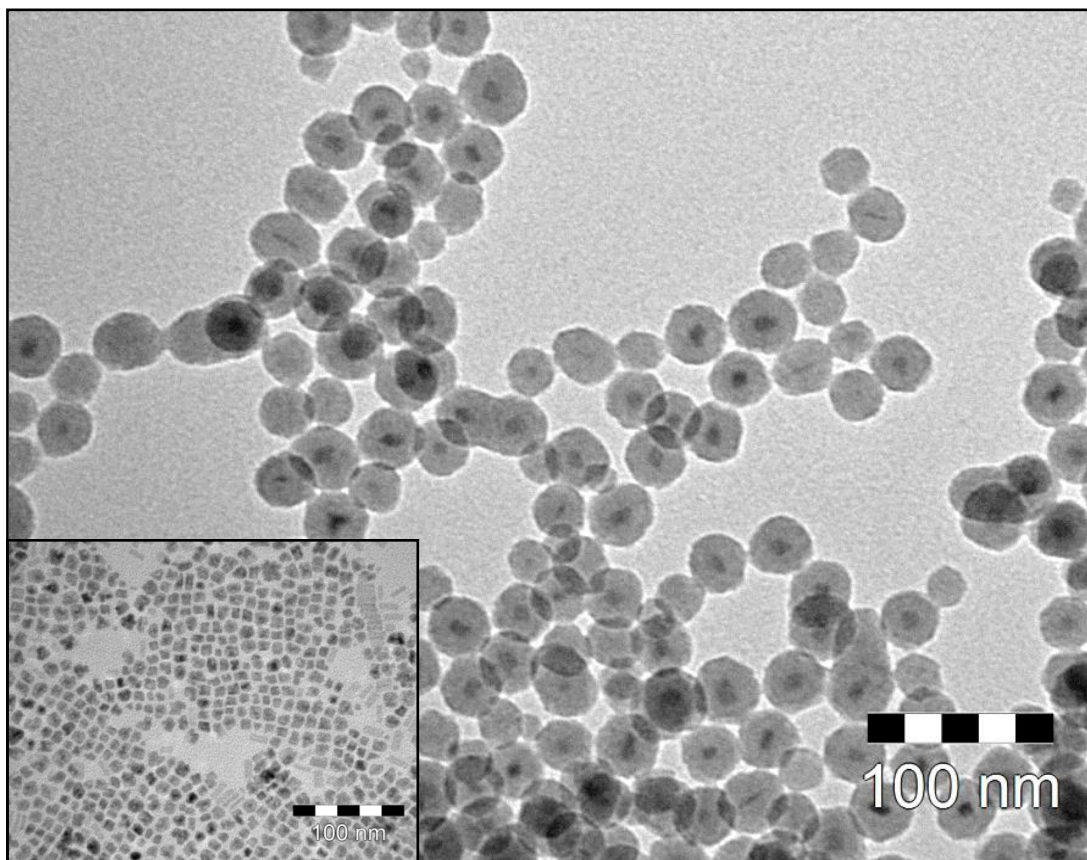
Cubic CdSe NCs, a side product of the CdSe NPLs prepared as described in 3.2.4, before (left corner) and after coating with silica in a microemulsion with 1.5 wt% ammonia in the aqueous phase, quenched after 3 hours of growth. These results confirm that NCs cubic in shape can be incorporated in silica with the reverse microemulsion. It is expected that, if a higher concentration of NCs is used in combination with a shorter growth time, thin uniform silica shells could be obtained around these CdSe cubes.